Investigating optical microplastic detection methods using fluorescent staining through Nile Red

by

Suparnamaaya Prasad

S.B Electrical Science and Engineering, S.B. Writing, MIT, 2022

Submitted to the Department of Mechanical Engineering
in partial fulfillment of the requirements for the degree of

MASTER OF SCIENCE IN MECHANICAL AND OCEAN ENGINEERING

at the

MASSACHUSETTS INSTITUTE OF TECHNOLOGY

May 2024

© 2024 Suparnamaaya Prasad. This work is licensed under a CC BY-NC-ND 4.0 license.

The author hereby grants to MIT a nonexclusive, worldwide, irrevocable, royalty-free license to exercise any and all rights under copyright, including to reproduce, preserve, distribute and publicly display copies of the thesis, or release the thesis under an open-access license.

Authored by:	Suparnamaaya Prasad Department of Mechanical Engineering May 20, 2024
Certified by:	Dr. Michael Triantafyllou Director of MIT Sea Grant, Thesis Supervisor
Certified by:	Dr. Andrew Bennett Learning and Curriculum Specialist, Thesis Supervisor
Accepted by:	Nicolas Hadjiconstantinou Chairman Department Committee on Graduate Theses

Investigating optical microplastic detection methods using fluorescent staining through Nile Red

by

Suparnamaaya Prasad

Submitted to the Department of Mechanical Engineering
on May 20, 2024 in partial fulfillment of the requirements for the degree of

MASTER OF SCIENCE IN MECHANICAL AND OCEAN ENGINEERING

ABSTRACT

Microplastics (MPs) are small pieces of plastic debris typically defined as smaller than 5mm. Given that the global environment faces a growing plastic pollution crisis, an urgent need exists for rapid, low-cost microplastic detection systems to characterize the health and environmental risk posed by MPs. Fluorescent tagging of microplastics using Nile Red (NR) has recently emerged as an accessible and popular detection method. However, robust, standardized methods of using Nile Red to identify between plastic and organic materials or distinguish between polymers are still being developed. This thesis pursued different optical microplastic detection methods using NR-based fluorescent staining with the ultimate goal of providing data that could be used towards building a polymer identification model that could be implemented into a low-cost detection system.

Three different investigations are presented. First, the fluorescence emission spectra of various plastic and organic samples stained with Nile Red is presented. The motivation behind this study was to identify the strongest fluorescence emission peaks for NR-stained plastics under a series of different excitation wavelengths. The spectral results provide a preliminary basis to distinguish Nile Red-stained plastics based on their fluorescent emission spectra alone. Second, this thesis presents a low-cost imaging set-up for fluorescent samples. The system applies the same excitation wavelengths and optical filters used to collect the spectral data. The images are then combined with the spectral data to illustrate another basis for rapidly distinguishing between different plastic polymers. Finally, an optical method for detecting microplastics in liquid samples using photodiodes is explored and discussed. Overall, this thesis contributes to the development of accessible microplastic detection technologies by leveraging the fluorescent properties of NR-stained plastics. The findings highlight the challenges and potential solutions for distinguishing between plastics and organic materials and distinguishing between different plastic polymers.

Thesis supervisor: Dr. Michael Triantafyllou
Title: Director of MIT Sea Grant

Thesis supervisor: Dr. Andrew Bennett
Title: Learning and Curriculum Specialist

Acknowledgments

I would like to express my deepest gratitude to my advisors, Dr. Michael Triantafyllou and Dr. Andrew Bennett, for their strong academic and professional support throughout graduate school. Their expertise and insights have been instrumental in shaping my journey as a researcher. I'm grateful for all that I've learned and all the ways I've grown during my time as a member of Sea Grant. I'd also like to thank members of the Sea Grant faculty for their invaluable guidance and encouragement. Thank you to Mike Sacarny, who never hesitated to help me with a project. Thank you to Dr. Carolina Bastidas and Rob Vincent for being great resources to ask questions. Additionally, I want to thank and acknowledge MIT.nano and DCIF for providing the necessary resources and facilities to conduct this research. I extend my gratitude to all those who contributed, directly or indirectly, to the completion of this thesis. Your support has been immensely appreciated.

Thank you to all of my friends and communities who helped me find balance in graduate school. Thank you to pika for being the most supportive living community I could wish for. I'm grateful to have lived in a magical, rainbow-colored home always filled with good food, laughter and music, and the best people. Thank you to all my friends from the MIT sailing team for all of the adventures. I'm especially grateful for my fellow Sea Grant lab mates and the good memories we've all shared together. Thank you to Annemarie, Fiona, Erin, Arianna, Sebastien and the countless others who transformed Sea Grant into a second home through your incredible friendship and support. An especially big thank you to my former lab mate Daniel for your unwavering confidence in me.

Lastly, a heartfelt thank you to my parents, Latha and Narasimha, and my younger sister Hima for the steady love and support always

Contents

Title page 1

Abstract 3

Acknowledgments 5

List of Figures 9

List of Tables 13

1 Introduction 15
- 1.1 Common Detection Techniques and Challenges . . . 16
  - 1.1.1 Nile Red . . . 17
  - 1.1.2 Photodetection . . . 18
  - 1.1.3 Automated Image Analysis . . . 18
  - 1.1.4 Counterstaining Method for Elimination of False Positives from Organic Materials . . . 19
- 1.2 General Approach . . . 20
- 1.3 Thesis outline . . . 20

2 Fluorescence Emission Spectra of Plastic and Organic Samples Stained with Nile Red 21
- 2.1 Motivation . . . 21
- 2.2 Methods . . . 22
  - 2.2.1 Reference materials and staining procedure . . . 22
  - 2.2.2 Fluorescence Spectrometer Set-Up . . . 24
- 2.3 Results and Discussion . . . 25
  - 2.3.1 Data Pre-Processing: Savitzky Golay Filter . . . 25
  - 2.3.2 Plastic Samples Stained with Nile Red . . . 25
  - 2.3.3 Organic Samples Stained with Nile Red . . . 30
  - 2.3.4 Preliminary Polymer Identification Scheme Based on Spectra from Nile Red-Stained Plastics . . . 34
  - 2.3.5 Field Trials . . . 36

2.4 Summary, Conclusions, and Prognosis . . . 38

3 Pairing spectral data with a low-cost microplastic imaging configuration for rapid polymer identification 39
3.1 Motivation . . . 39
3.2 Imaging Methods . . . 40
3.2.1 Fluorescence Imaging System Set-Up and Image Collection . . . 40
3.3 Results and Discussion . . . 42
3.3.1 Nile Red Stained Plastic Samples . . . 44
3.4 Conclusion and Future Work . . . 52

4 Utilizing low-cost photodiodes for microplastic detection in liquid samples 53
4.1 Motivation . . . 53
4.2 Materials and Methods . . . 55
4.2.1 Chemicals . . . 55
4.2.2 Experimental Procedure . . . 58
4.3 Results and Discussion . . . 59
4.4 Conclusions and Future Work . . . 64

5 Summary, Conclusions, and Prognosis 67
5.1 Fluorescence Emission Spectra for Nile Red stained Plastics . . . 67
5.2 Pairing spectral data with a low-cost microplastic imaging configuration for rapid polymer identification . . . 68
5.3 Utilizing low-cost photodiodes for microplastic detection in liquid samples . . . 68
5.4 Final Conclusion . . . 68

A Fourier Transform Infrared Spectroscopy (FTIR) Results for Polymer Validation 69

References 85

List of Figures

2.1 Schematic of the measurement of emission spectra in a spectrofluorometer . 24

2.2 Fluorescent emission peaks of plastic samples stained with Nile Red and excited at 405 nm. PE, PS, PP, Nylon, and PVC generally share peaks at 485 nm, 529 nm, and 552 nm. Nylon, PUR, and PVC possess additional fluorescence from 580 nm to 650 nm. Polyester has no discernible peaks aside from roughly 469 nm due to high levels of autofluorescence. 26

2.3 Fluorescent emission peaks of plastic samples stained with Nile Red and excited at 465nm. PE and PP share similar spectra with peaks at approximately 542 nm, 57 3nm, and 634 nm. PS and PVC have peaks in the 560 nm-580 nm range. Nylon, polyester, and PUR have peaks in the 600 nm-620 nm range. Based on the area under the normalized intensity curves, PE and PP appear to be less fluorescent than the other plastics with broad emission curves. . . 28

2.4 Fluorescent emission peaks of plastic samples stained with Nile Red and excited at 525nm. The spectra of the plastics all emit a broad and smooth emission curve. The peak wavelengths are within roughly 40 nm of each other. 29

2.5 The majority of the organic materials characterized possess peaks around 485 nm and 552 nm. Wool and cotton exhibit additional fluorescence in the 600nm to 650 nm range. Silk carries some measure of autofluorescence that overpowers other spectral peaks. 31

2.6 Chitin and wood possess similar peaks near 542 nm and 634 nm. Cotton, silk, and wool appear slightly more red-shifted in comparison to hemp. 32

2.7 The spectra of the plastics all emit a broad emission curve with most organic samples exhibiting peak fluorescence between 605 nm and 621 nm. 33

2.8 This polymer identification flowchart is based on the spectra collected from plastics stained with Nile Red. From the current dataset, it is difficult to find spectral characteristics that could further identify PE from PP and Nylon, PUR, and PVC from each other. Therefore, this process flow is conservative and intended as a preliminary interpretation of the spectral characteristics presented in this chapter. The next step is to encode and test this identification process within an automated tool that can extract and match spectral peaks to a standardized database. 35

2.9 This graph displays the fluorescent spectra of 5 polypropylene field samples and 3 polyethylene samples for excitation at 405 nm, 465 nm, and 525 nm. Four polypropylene samples and all polyethylene samples share all spectral peaks for 405 nm and 465 nm excitation. For 525 nm excitation, the polyethylene samples contain no visible peaks, which indicates that the long-pass filter may have restricted the spectral window. 37

3.1 The system excites a sample with blue light (left) and green light (right). An adjustable mount allows the user to raise and lower the camera to adjust focus. A long pass filter with a 570 nm cut-on wavelength can be seen fixtured below the camera. 42

3.2 Fragments from seven plastics stained with Nile Red are depicted. Similar to the spectral data recorded in Chapter 2 for NR-stained plastics, the strongest fluorescent intensity for several plastics is elicited by a 525 nm excitation wavelength with a 570 nm cut-on filter or 405 nm (in the case of Polyester's strong autofluorescence) with a 455 nm cut-on filter. The weakest excitation wavelength and filter combination appears to be 405 nm excitation with a 570 nm cut-on filter. 43

3.3 Nile Red-stained polyethylene is excited at wavelengths 405 nm, 465 nm, and 525 nm. PE experiences its two strongest emission intensities when excited by 405nm. Correspondingly, the two brightest images of PE in Figure [3.2] were both taken using the 405nm excitation wavelength (one image used the 455 nm filter and the other 530 nm). These cropped images are visibly brighter than those depicting PE excited by either 465 nm or 525 nm excitation wavelengths. 45

3.4 Nile Red-stained polystyrene is excited at wavelengths 405 nm, 465 nm, and 525 nm. PS appears the brightest when using a 525 nm excitation wavelength and 570 nm filter. This fits well with the spectra data given that the peak emission intensity is approximately 590 nm with a 525 nm excitation. 46

3.5 Nile Red-stained polypropylene when excited at wavelengths 405 nm, 465 nm, and 525 nm. Visually, the peaks excited by 465 nm and 525 nm seem equally bright, and their spectral peaks are similarly close. The peak excited by 405 nm is noticeably dimmer, both visually and graphically. 47

3.6 Nile Red-stained nylon is excited at wavelengths 405 nm, 465 nm, and 525 nm. Visually, nylon is the brightest when excited at 525 nm and photographed through the 570 nm filter. This aligns well graphically, where Nylon's highest emission peak is located near 610 nm with an excitation wavelength of 525 nm. The dimmed appearances of Nylon excited by 405 nm and 465 nm in comparison to 525 nm match the graphed spectra. 48

3.7 Nile Red-stained polyester is excited at wavelengths 405 nm, 465 nm, and 525 nm. From the images, Polyester is strongly fluorescent when excited by 405 nm and seen through a 455 filter. When excited by 525 nm, red-tinted Polyester can be faintly seen, while little to no fluorescence can be seen at all for 465 nm excitation. These results match the graphed relative intensity peaks. 49
3.8 Nile Red-stained polyurethane is excited at wavelengths 405 nm, 465 nm, and 525 nm. The cropped images from Figure [3.2] are visually brightest at 525 nm excitation, and progressively less bright at 465 nm and 405 nm excitation, respectively. These visual characteristics match the highest spectral emission intensity peak at approximately 625 nm when excited by 525 nm. 50
3.9 Nile Red-stained polyvinyl chloride is excited at wavelengths 405 nm, 465 nm, and 525 nm. PVC is visually brightest with a 525 nm excitation, similar to the highest emission intensity peak at 525 nm within the spectra. 51

4.1 This figure presents a top view of the experimental set-up (not drawn to scale). Blue light from the LEDs excites the microplastics in the cuvette, causing them to fluoresce. Fluorescing light passes through the long pass filter (which eliminates the blue LED light) and is then focused by the plano-convex lens into the photodiode receptor. 56
4.2 This figure presents images taken of the experimental set-up. A custom rig was 3D printed to hold and position the system components. 57
4.3 This figure presents the circuit schematic used in the optical detection system. An RC configuration acts as a noise filter. A large value was chosen for R_L based on Equation 1. 57
4.4 Unamplified signal output in mV versus microplastic concentration. Each data series represents a different solution concentration of Nile Red. Trend lines show a strong linear fit for the unamplified data. 60
4.5 This figure presents 10x amplified signal output in mV versus microplastic concentration. Each data series represents a different solution concentration of Nile Red. Compared to the unamplified data, 10x amplification still provides a linear fit with minimal introduction of noise. 61
4.6 This figure presents a 100x amplified signal output in V versus microplastic concentration. Each data series represents a different solution concentration of Nile Red. Compared to the unamplified data, 100x amplification introduces noticeable noise for NR concentrations of 1 ug/mL and 2 ug/mL. Given the increased noise in the amplified data and the similar linear trend lines across amplification settings, an external amplifier such as the SR560 pre-amplifier may not be necessary or can be substituted for a transimpedance amplifier circuit. 62

4.7 Control and fluorescing test solutions for various microplastic and Nile Red concentrations. Little yellow-green fluorescent light can be seen in control solutions, even with higher MP concentrations. The 1 ug/mL and 2 ug/mL solutions present similar visual fluorescence characteristics. The 3 ug/mL is generally brighter across each MP concentration. A slight red tinge can also be seen in these solutions due to excess dye in the liquid sample. 63

A.1 FTIR spectra for polypropylene 69
A.2 FTIR spectra for polyethylene 70
A.3 FTIR spectra for polystyrene 71
A.4 FTIR spectra for polyester 72
A.5 FTIR spectra for polyurethane 73
A.6 FTIR spectra for polyvinyl chloride 74
A.7 FTIR spectra for nylon 75
A.8 FTIR spectra for polypropylene field sample 1 76
A.9 FTIR spectra for polypropylene field sample 2 77
A.10 FTIR spectra for polypropylene field sample 3 78
A.11 FTIR spectra for polypropylene field sample 4 79
A.12 FTIR spectra for polypropylene field sample 5 80
A.13 FTIR spectra for polyethylene field sample 1 81
A.14 FTIR spectra for polyethylene field sample 2 82
A.15 FTIR spectra for polyethylene field sample 3 83

List of Tables

2.1 Sample Material Table 23

Chapter 1

Introduction

Global plastic pollution is a rising environmental crisis. In 2019, annual plastic waste was estimated to be 353 million tons [1]. By 2060, over 1000 million tons are estimated to be in the natural environment. Plastics became a staple ingredient in many consumer products during the post-World War II period due to their extreme versatility, durable nature, low cost, and ease of manufacturing. However, most plastics are extracted from fossil fuels such as crude oil, natural gas, and coal, which are then refined and polymerized to form raw plastics [2]. Furthermore, plastics have a prolonged biodegradation period, ranging from decades to millennia. Without a global strategy for managing end-of-life plastics, most plastic ever produced still exists in some shape or form.

The International Union for Conservation of Nature (IUCN) reports that over 10 million tons of plastic enter our oceans annually [3]. Their environmental impact is staggering compared to natural disasters like the Deepwater Horizon oil spill, which released over 560,000 tons of oil [4]. The IUCN also estimated that plastic makes up 80% of all marine debris found, ranging from surface waters to deep-sea sediments [3]. Goal 4 of the National Oceanic and Atmospheric Administration (NOAA) Marine Debris Program is focused on the Monitoring and Detection of Marine Debris, intending to generate and share marine debris detection and shoreline monitoring data, products, and guidance to inform decision-making. "Life Below

Water" is the focus of the United Nations' Sustainable Development Goal (SDG), with the target of SDG 14.1 "to prevent and significantly reduce marine pollution of all kinds, in particular from land-based activities, including marine debris and nutrient pollution." Clearly, the consequences of marine pollution are a focus of growing global concern.

Plastics easily disperse in the marine environment due to their lightweight and durable nature. Ultraviolet radiation and other environmental forces break down plastic pollutants into micro and nano-sized fragments ranging from less than 0.1um in size to greater than 25mm. While rigid size classification standards for plastic pollutants are not internationally agreed upon, fragments that are between 0.1um to 5 mm are generally referred to as microplastics (MPs), and fragments less than 0.1um are generally referred to as nanoplastics (NPs). Due to their diminutive size, fragmented plastics have propagated through marine ecosystems and been detected in remote regions such as Arctic sea ice and the Marianna Trench and found within the digestive tracts of marine life ranging from zooplankton to whales. Rapidly detecting and quantifying MPs is necessary to accurately assess the health and environmental hazards posed by plastic proliferation in the environment.

1.1 Common Detection Techniques and Challenges

At the beginning of the project, a literature review of state-of-the-art microplastic detection techniques was conducted. There is currently no standard detection and analysis process for microplastics, and often a suite of instruments are utilized to achieve plastic identification. Characterizing the presence of MPs in the marine environment requires quantifying MP concentration and polymer makeup. However, consumer plastic products found in the ocean are often the product of additives such as colorants, stabilizers, reinforcements, and plasticizers, alongside the polymer constituent. Such additives often affect plastic pollutants' visual appearance and degradation rate. This leads to immense variety among plastic particles regarding size, shape, appearance, and other material characteristics, making detection dif-

ficult to standardize. Common detection methods include visual analysis through the naked eye or fluorescence microscopy, Fourier Transform Infrared Spectroscopy (FTIR), Raman Spectroscopy, and pyrolysis gas chromatography-mass spectrometry (Py-GC-MS). While visual analysis is often the easiest to perform, it does not provide data on the sample's chemical composition and is prone to inaccuracies for small particles. On the other hand, FTIR provides detailed information on chemical bonds and functional groups within samples, making it ideal for qualitative detection and compositional analysis of microplastics. However, its effectiveness is limited to particles larger than 20 µm. Raman Spectroscopy operates on the principle of inelastic light scattering and generates a spectral fingerprint unique to the material analyzed. This technique can identify microplastics below 20 µm without requiring sample drying or dehydration, but the efficiency is still hampered by long detection times. Thermal analysis techniques such as Py-GC-MS identify microplastic composition and type based on specific thermal signatures through sample heating. However, the destructive nature of this method makes it unsuitable for assessing physical properties like appearance and morphology, which can be an important characteristic to assess in microplastic detection surveys [5]. The downside to each spectroscopy and spectrometry technique is the cost of lab equipment, which can be prohibitive for financially constrained research communities interested in microplastic detection. Therefore, a need exists for a rapid, low-cost microplastic detection system that can be accessed and deployed by a range of coastal communities. The thesis focuses on addressing this problem by providing data and proof-of-concept configurations to build robust, low-cost, and portable detection systems.

1.1.1 Nile Red

An emerging optical-based microplastic detection technique using the fluorescent dye Nile Red (NR) is growing in popularity after a 2017 Nature publication by Maes et. al (2017) which demonstrated a high recovery rate of NR-dyed microplastics from spiked sediment samples. Nile Red is a hydrophobic dye that exhibits little fluorescence in water and binds

preferentially to plastics due to its lipophilic properties. Furthermore, the fluorescence emissions from NR-dyed plastics shift in color and intensity based on the plastic polymer, ranging from yellow to deep red. Maes et. al (2017) noted that the solvatochromatic properties of the dye could be leveraged for plastic categorization based on polymer surface polarity [6]. Nile Red is also not costly; fluorescent emissions can be detected through low-cost photodiodes or cameras. Studies have also indicated that Nile Red stains organic material slower than plastics, a property that can potentially reduce false positives in environmental samples. Together, these characteristics make Nile Red ideal for low-cost, field-portable microplastic detection applications by combining the ease of visual analysis with insight into chemical composition at an inexpensive cost. Based on these promising features, fluorescent emission detection using Nile Red was selected as the optical detection method for this thesis project.

1.1.2 Photodetection

Detecting fluorescent emissions of Nile Red-stained plastics through optical light detection methods is still a novel field. Bianco et. al (2023) combined flow cytometry and dye-staining to detect NR-stained plastic particles by measuring dynamic light scattering [7]. While their method performed well using laboratory-prepared suspensions, testing a complex organic matrix showed that interactions between organic matter and plastic particles may negatively impact the accuracy. Furthermore, combining flow cytometry with dye staining proved ineffective in detecting plastic particles functionalized with hydrophilic functions. While flow cytometry can be costly, measuring fluorescent emissions of dyed plastics using light sensors or inexpensive photodetectors can be accomplished as part of a low-cost application.

1.1.3 Automated Image Analysis

Automated image analysis methods of microplastic detection using Nile Red have been explored. Meyers et. al (2022) detail a semi-automated approach using a machine-learning model capable of microplastic classification based on their RGB profiles [8]. While their

model successfully distinguished plastics from organic material and classified polymer type, their model was trained and validated on high-quality images obtained with fluorescence microscopy. Their work holds the potential for adaptation to a low-cost approach. Still, an in-situ or field-portable application will need to be retrained on images taken with a field-portable camera, not a fluorescence microscope. This can negatively impact the accuracy of the model in distinguishing between plastics and non-plastics, indicating that another approach to reduce false negatives needs to be integrated. Similarly, Sturm et. al (2023) developed an automated microplastic imaging method using Nile Red stained plastic particles for deployment in wastewater plants. While their methodology required digestion to eliminate false positives caused by organic samples, the highest costs of their experimental setup were attributed to fluorescence microscopy [9]. If inexpensive images can be used to train a similar model, this method can be considered viable for low-cost applications in conjunction with methods to eliminate false positives.

1.1.4 Counterstaining Method for Elimination of False Positives from Organic Materials

Furthermore, studies have warned that Nile Red staining methods can lead to false positives due to dye uptake by biological material or clumps of dye aggregates across a sample surface or within liquid, leading to overestimating microplastic particles [10]–[13]. One approach to reducing false positives caused by biological materials is counterstaining samples already stained by Nile Red with a different fluorescent dye that exclusively binds to biological materials. Counterstaining approaches with Nile Red have been explored using dyes such as Calcofluor White, Evans Blue, or DAPI [14], [15]. However, literature using fluorescence spectroscopy to characterize the fluorescence emission spectra of particles stained with Nile Red and a counterstain is scarce. Nile Red is a solvatochromatic dye, meaning that its emission color will shift based on the polarity of the surface it stains. Given that the introduction of another fluorescent stain can influence the polarity of the Nile Red stained

plastics, it's critical to understand which plastic polymers are the most suitable to be detected using a counterstaining method.

1.2 General Approach

Based on the literature review, three methods of microplastic detection were explored. First, the fluorescent emission spectra of Nile Red-stained materials were characterized using a fluorescent spectrometer for three different excitation wavelengths. Second, the spectral data was used to inform a proof-of-concept low-cost visual detection system utilizing a Raspberry Pi camera. Third, MP detection was explored in liquid samples through fluorescence emission detection with photodiodes. A benchtop system was built and tested as a proof-of-concept.

1.3 Thesis outline

Chapter 2 presents fluorimetry data collected from NR-stained plastics and organic material. Chapter 3 presents a low-cost imaging set-up for fluorescent samples that uses spectral data to distinguish between different plastic polymers. Chapter 4 uses photodiodes as the basis of an MP detection method for plastics in liquid samples. Chapter 5 presents summary, conclusion, and future work.

Chapter 2

Fluorescence Emission Spectra of Plastic and Organic Samples Stained with Nile Red

This thesis aims to provide data on Nile Red-based optical microplastic detection methods that can eventually be applied to low-cost, field portable microplastic detection systems. This chapter presents fluorescent emission spectra for plastic and organic matter dyed with Nile Red (NR). A fluorescence emission spectral dataset was collected to build a rapid polymer identification scheme for future field-deployable systems.

2.1 Motivation

As introduced in Chapter 1, microplastic detection poses several challenges due to the range of shape, density, physical degradation, additives, and chemical composition of plastics found in the natural environment. Classical methods such as Fourier transform infrared spectroscopy (FTIR) and Raman spectroscopy are complex, expensive, and time-consuming [16]. Fluorescent tagging using solvatochromatic dyes to stain plastics has emerged as a low-cost, accessible approach. A particular solvatochromatic dye, Nile Red, has recently emerged as

the most efficient dye in staining plastics by several studies [6], [17]–[20]. However, fluorescent staining methods using Nile Red are not yet standardized; a literature review reveals a range of solvent choices for Nile Red, staining protocols, excitation wavelengths for stained plastics, and optical filters for experimental set-ups [21]. Identifying the strongest fluorescence emission peaks for Nile Red-stained plastics for various excitation wavelengths will further refine experimental configurations. Excitation wavelengths and optical filters can be consistently selected to maximize plastic fluorescence intensity. Furthermore, measuring spectra for multiple excitation wavelengths can reveal key spectral patterns for a polymer identification model.

Several studies have provided the fluorescence emission spectra for unstained plastics or select Nile Red-stained plastics at a single excitation wavelength, typically within the UV range [13], [17], [22]–[24]. However, finding a comprehensive plastic dataset using multiple excitation wavelengths was difficult. Therefore, this study was designed to have three different excitation wavelengths per plastic sample to maximize spectral data.

2.2 Methods

2.2.1 Reference materials and staining procedure

Table [2.1] shows all sample materials used in this study. This study used seven commercially available plastics: polypropylene (PP), polyethylene (PE), polystyrene (PS), polyester, polyurethane (PUR), polyvinyl chloride (PVC), and nylon. These polymers were chosen because they're commonly found in the marine environment and contain a range of densities. The plastics were purchased from McMaster-Carr, and the polymer composition types were verified using a Bruker Alpha II FTIR spectrometer (see A.1-A.7). All spectra were recorded in transmittance mode in the infrared spectral range 4000-400 cm^{-1} using a resolution of 4 cm^{-1} and 64 scans per sample. The recorded spectra were then compared with commercial spectra libraries for verification.

Chitin, hemp, wool, wood (birchwood), silk, and cotton were used as representative organic samples. The natural textile fibers were purchased online. These materials were chosen because they are commonly mistaken for plastic fragments or fibers, and they have also been used in other published studies exploring microplastic detection methods.

Before fluorimeter processing, materials were cut or shaped into roughly 30 mm x 30 mm sample sizes. The samples were washed with Milli-Q water and vacuum-filtered onto Whatman glass filters. After drying, a 10 g/mL acetone Nile Red solution was pipetted onto the samples. After 15 minutes, the samples were washed with Milli-Q water to remove residual dye. All solutions and suspensions were prepared using Milli-Q water.

Material	**Source**	**Form Factor**	**FTIR Spectra**
Polypropylene (PP)	McMaster-Carr	Translucent sheet	A.1
Polyethylene (PE)	McMaster-Carr	White sheet	A.2
Polystyrene (PS)	McMaster-Carr	White sheet	A.3
Polyester	Craft store stuffing/fill	Fiber	A.4
Polyurethane (PUR)	McMaster-Carr	White foam	A.5
Polyvinyl Chloride (PVC)	McMaster-Carr	White pipe	A.6
Nylon	McMaster-Carr	Translucent sheet	A.7
Chitin	Grocery store shrimp	Dried shrimp	NA
Wood	Craft store	Popsicle sticks	NA
Hemp	Craft store stuffing/fill	Fiber	NA
Wool	Craft store stuffing/fill	Fiber	NA
Silk	Craft store stuffing/fill	Fiber	NA
Cotton	Craft store stuffing/fill	Fiber	NA

Table 2.1: Sample Material Table

2.2.2 Fluorescence Spectrometer Set-Up

A fluorescence spectrometer, or fluorimeter, fully characterized the emission wavelength peaks of organic and plastic particles stained with Nile Red (NR). Fluorimetry is a form of optical spectroscopy that excites a sample with light and measures the resulting fluorescence. In this experiment, the system used fixed excitation wavelengths to excite the dyed samples and record the resulting emission spectral peaks. Figure 2.1 displays an infographic that describes data collection for emission spectra in a fluorescence spectrometer.

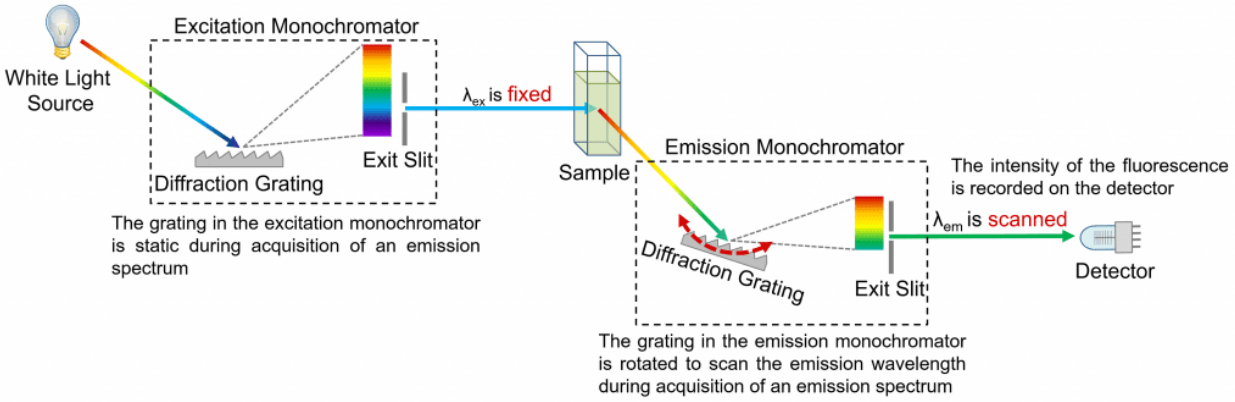

Figure 2.1: Schematic of the measurement of emission spectra in a spectrofluorometer [25]

For spectral data collection, a Cary Eclipse fluorescence spectrometer equipped with a Xenon flash lamp was used. Sample excitation was recorded for three different wavelengths: 405 nm, 465 nm, and 525 nm, which are commonly used to excite Nile Red. Furthermore, these wavelengths can also easily be found in commercially available and low-cost light sources through ultra-violet (UV), blue, and green LEDs, respectively.

To filter excitation light from the fluorescence spectrometer, long pass filters made from Schott glass with cut-on wavelengths of 455 nm (Edmund Optics SCHOTT GG455), 530 nm (Edmund Optics SCHOTT OG530), and 570 nm (Edmund Optics SCHOTT OG570) were used for 405 nm, 465 nm, and 525 nm excitation wavelengths respectively. The voltmeter sensitivity was adjusted for each sample to increase excitation peak separation. The wavelength range of 460 nm -700 nm was scanned for spectral peaks excited by 405 nm, the

wavelength range of 535 nm -700 nm was scanned for spectral peaks excited by 465 nm, and the wavelength range of 570 nm - 700 nm was scanned for spectral peaks excited by 525 nm. These distances were chosen because the long pass filters did not sharply filter out the excitation light caused by the Xenon lamp (white light source). A scan rate of 600 nm/min, a data interval of 1 nm, and an averaging time of 0.1 seconds were used. The excitation and emission slits were set to 5 nm.

2.3 Results and Discussion

2.3.1 Data Pre-Processing: Savitzky Golay Filter

The following section presents the fluorimeter results. The raw results were first processed using the Savitzky-Golay smoothing method. Smoothing is commonly used on spectral data to reduce noise and isolate key spectral features that may otherwise be obscured. The Savitzky-Golay selects a window around each data point in a spectrum and fits a polynomial to the points within the window. The data point is then replaced with the value of the fitted polynomial. For the data presented in this thesis, a window size of 11nm and a polynomial order of 3 was used. The intensity was normalized to values from 0 to 1. The data was then plotted in MATLAB, and a peak finder algorithm was used to label prominent peaks.

2.3.2 Plastic Samples Stained with Nile Red

The fluorescent emission peaks of plastic samples stained with NR are shown in Figures [2.2], [2.3], and [2.4]. Figure [2.2] depicts plastics excited at 405 nm. Some plastics exhibit autofluorescence at this wavelength, most notably polyester. From the spectra collected, the plastics (save for polyester) all exhibit fluorescent peaks at 485 nm and 552 nm. Nylon, PUR, and PVC also exhibit 580 to 650 nm fluorescence. These latter spectral peaks can be distinguishing factors for a polymer identification model.

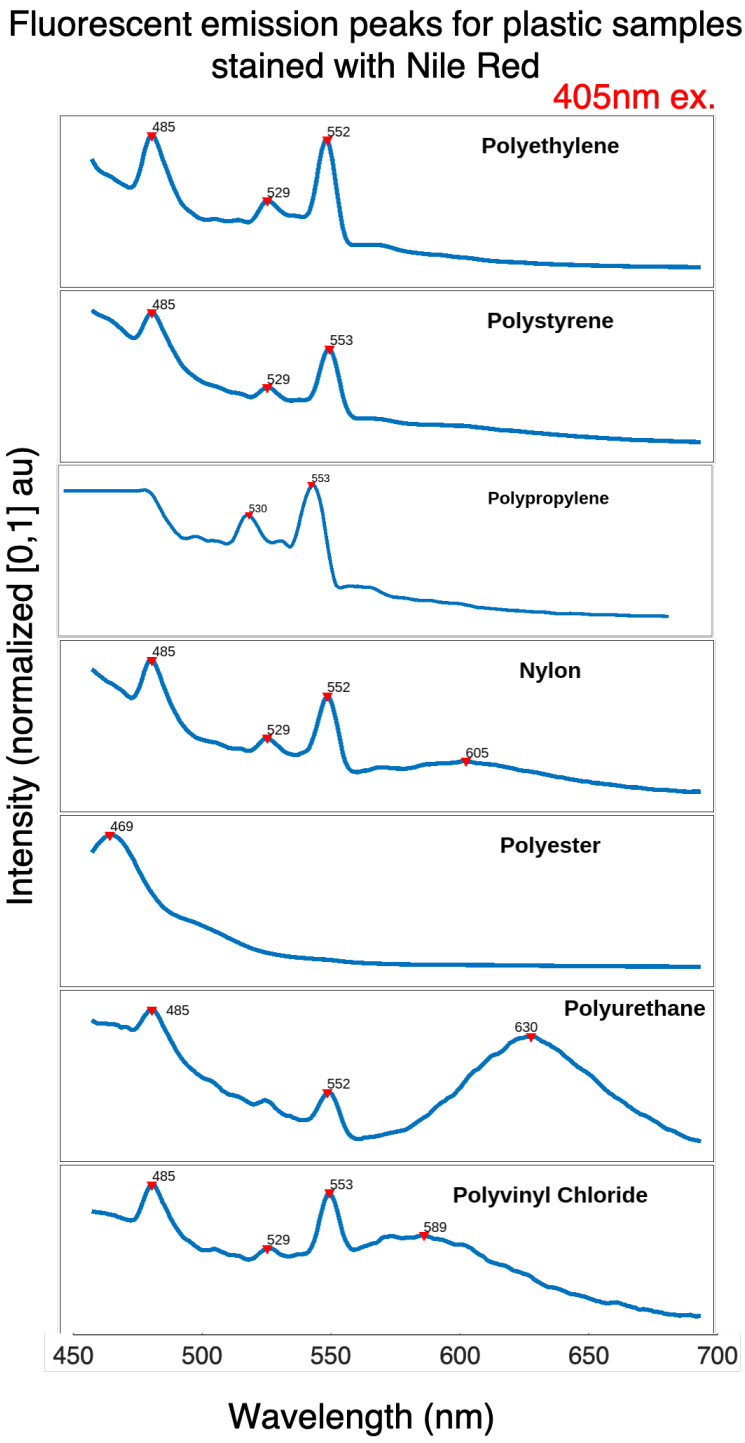

Figure 2.2: Fluorescent emission peaks of plastic samples stained with Nile Red and excited at 405 nm. PE, PS, PP, Nylon, and PVC generally share peaks at 485 nm, 529 nm, and 552 nm. Nylon, PUR, and PVC possess additional fluorescence from 580 nm to 650 nm. Polyester has no discernible peaks aside from roughly 469 nm due to high levels of autofluorescence.

Figure [2.3] depicts plastics excited at 465nm. PE and PP share similar spectra at this excitation wavelength and possess excitation peaks at roughly 541 nm, 572 nm, and 633 nm. The peaks decrease in intensity with wavelength. PS, PVC, Nylon, Polyester, and PUR all possess more fluorescence intensity in the 550 nm to 650 nm region. PS and PVC have peaks between 560 nm and 580 nm while Nylon, Polyester, and PUR contain more red-shifted peaks.

Figure [2.4] portrays plastics excited at 525nm. The plastics do not have sharp distinguishing characteristics at this excitation wavelength in their spectra. PS, Nylon, Polyester, and PUR contain more right-shifted peaks than PE, PP, and PVC.

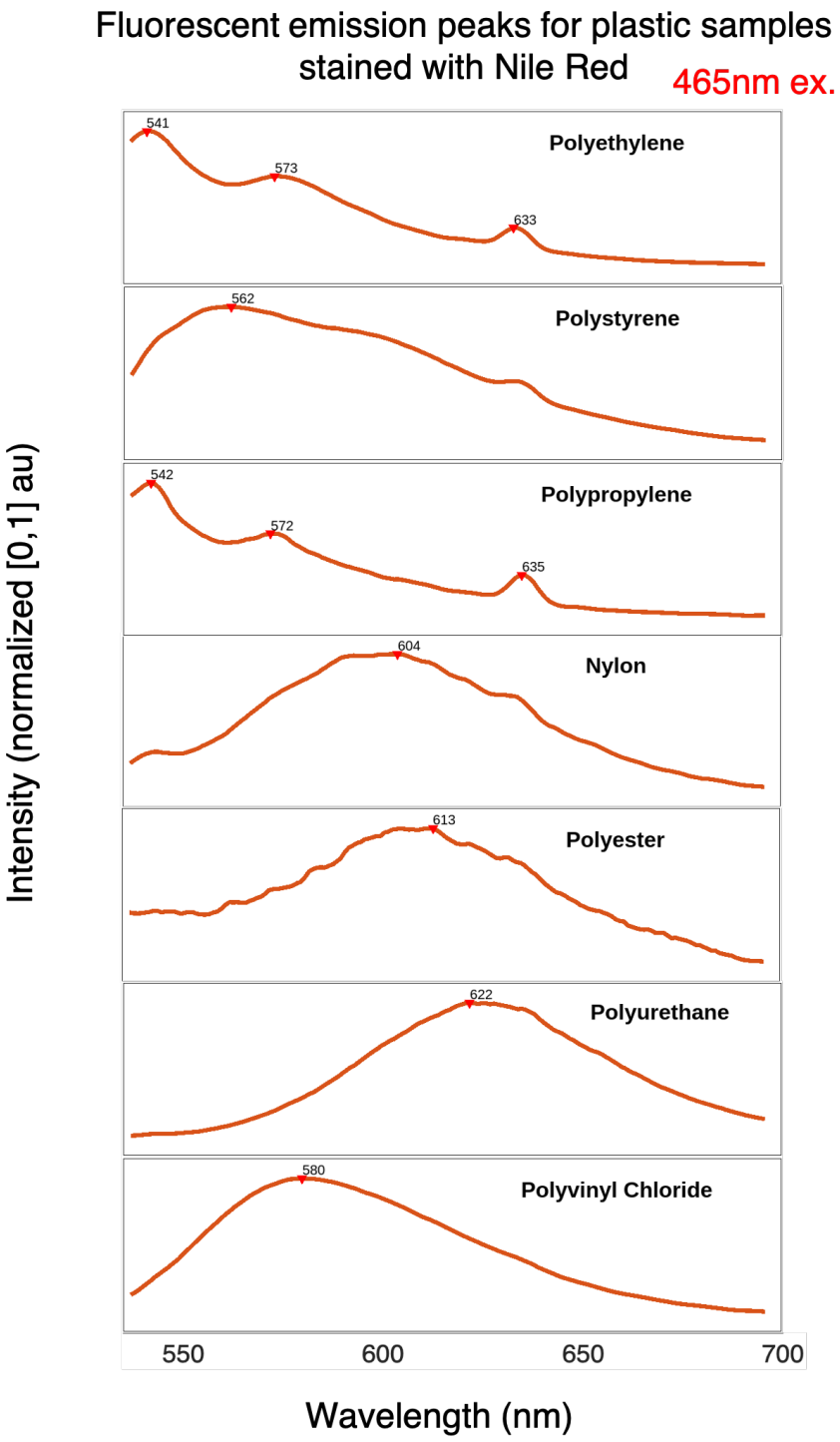

Figure 2.3: Fluorescent emission peaks of plastic samples stained with Nile Red and excited at 465nm. PE and PP share similar spectra with peaks at approximately 542 nm, 57 3nm, and 634 nm. PS and PVC have peaks in the 560 nm-580 nm range. Nylon, polyester, and PUR have peaks in the 600 nm-620 nm range. Based on the area under the normalized intensity curves, PE and PP appear to be less fluorescent than the other plastics with broad emission curves.

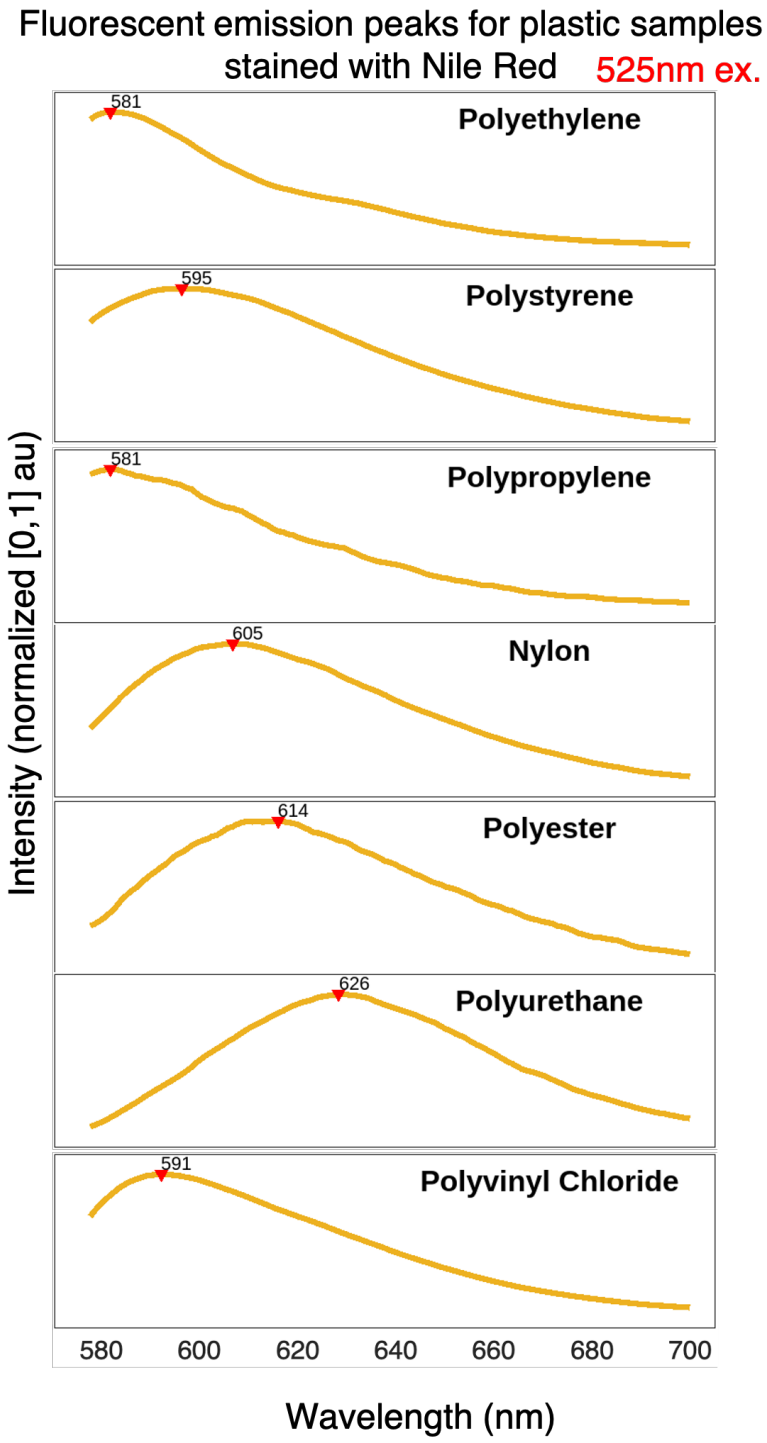

Figure 2.4: Fluorescent emission peaks of plastic samples stained with Nile Red and excited at 525nm. The spectra of the plastics all emit a broad and smooth emission curve. The peak wavelengths are within roughly 40 nm of each other.

2.3.3 Organic Samples Stained with Nile Red

The fluorescent emission peaks of organic samples stained with Nile Red are shown in Figures [2.5], [2.6], and [2.7]. The data shows that the stained organic samples generally exhibit similar spectral characteristics to Nile Red-stained plastic samples based on excitation wavelength. For a 405 nm excitation wavelength, wood, wool, hemp, cotton, and chitin all exhibit peaks near 485 nm and 553 nm. This spectra is remarkably similar to the the spectra of PP and PE presented in Figures [2.2]. However, only chitin and wood presented spectra similar to PP and PE when excited by 465 nm. When excited by 525 nm, chitin and wood possess spectral peaks that are red-shifted in comparison to that of PP and PE. While this indicates that optical filtering based on spectral peaks of Nile Red stained samples may not reliably eliminate false positives, combining spectral peaks across different wavelengths paints a fuller picture of the material.

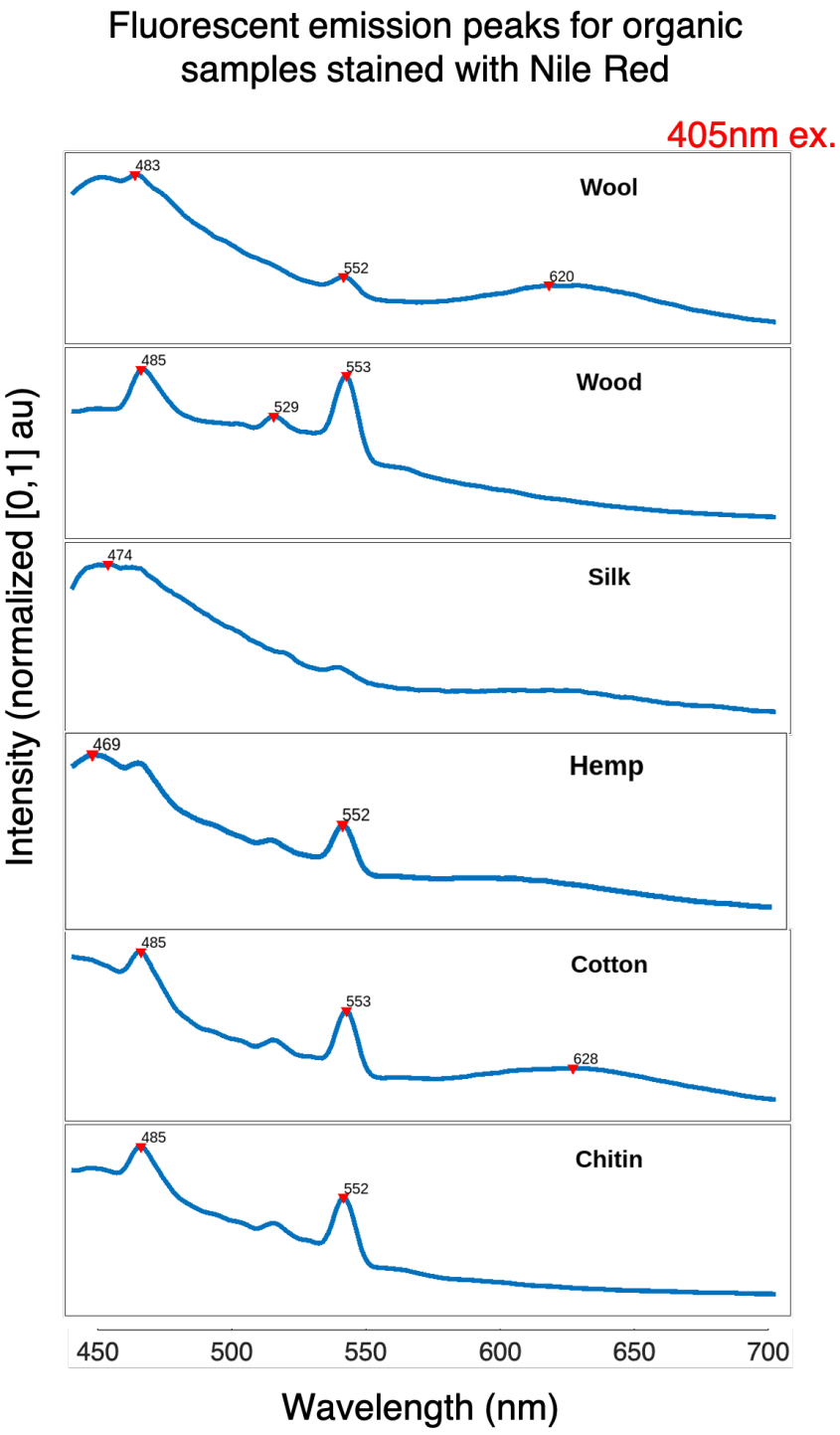

Figure 2.5: The majority of the organic materials characterized possess peaks around 485 nm and 552 nm. Wool and cotton exhibit additional fluorescence in the 600nm to 650 nm range. Silk carries some measure of autofluorescence that overpowers other spectral peaks.

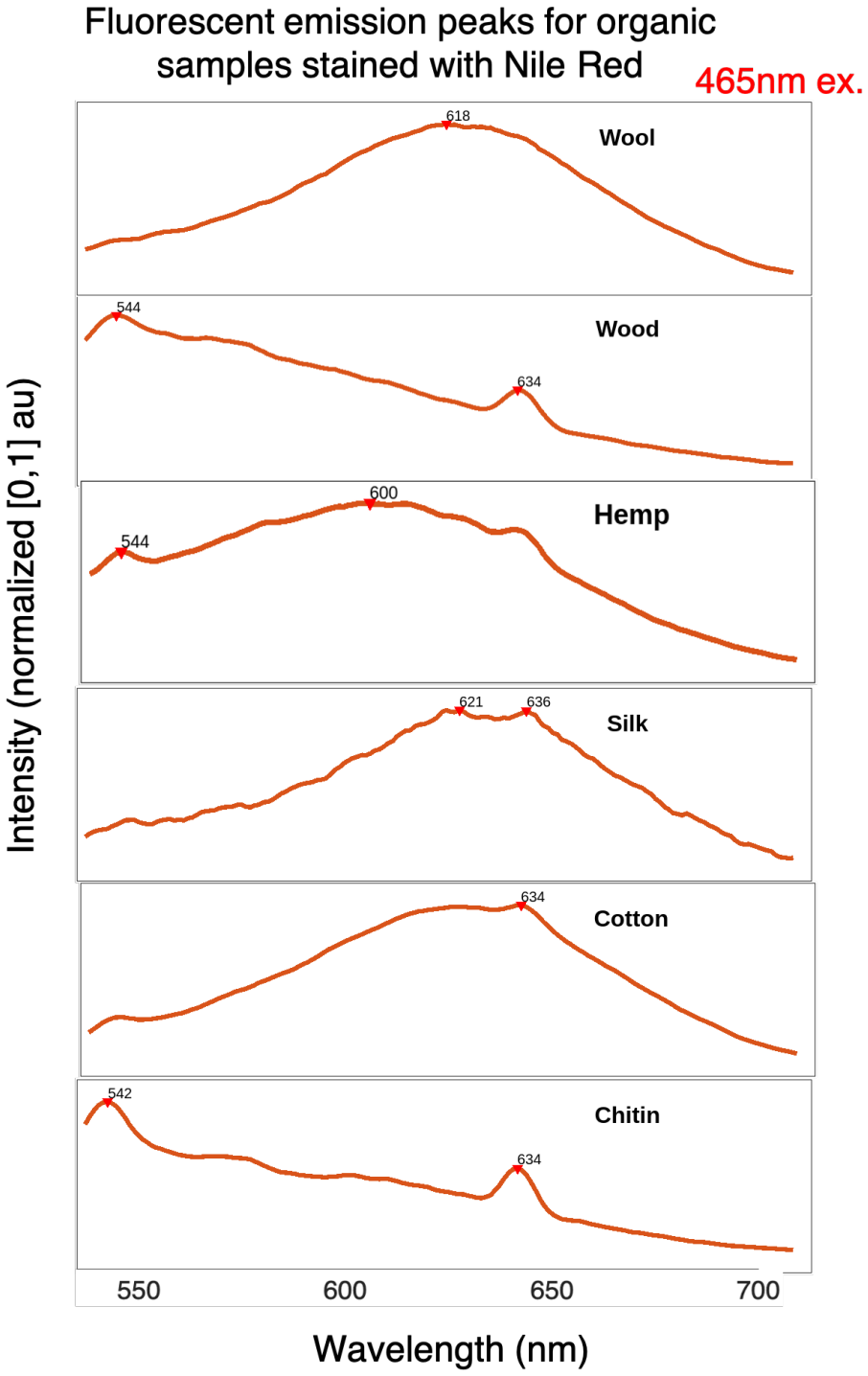

Figure 2.6: Chitin and wood possess similar peaks near 542 nm and 634 nm. Cotton, silk, and wool appear slightly more red-shifted in comparison to hemp.

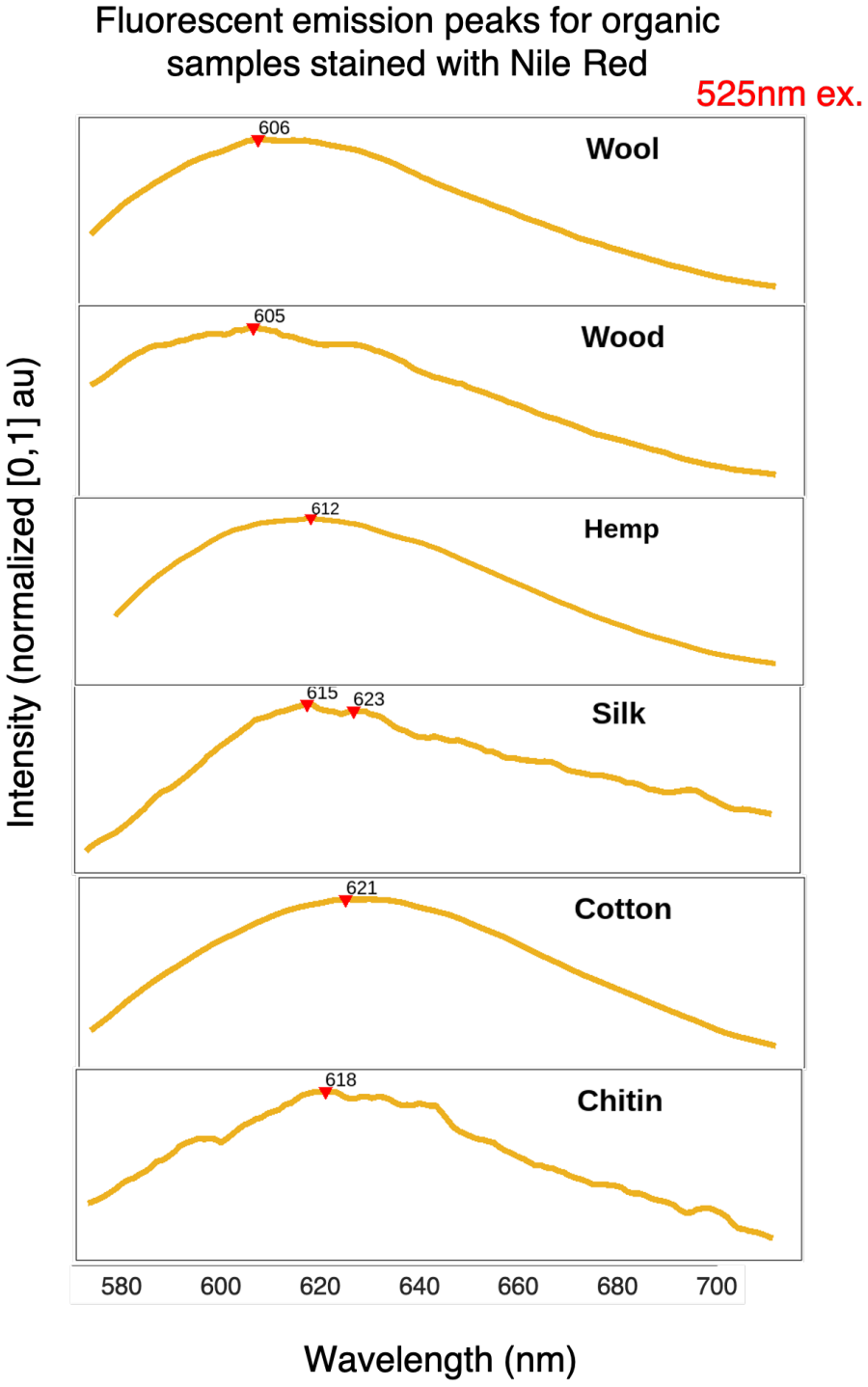

Figure 2.7: The spectra of the plastics all emit a broad emission curve with most organic samples exhibiting peak fluorescence between 605 nm and 621 nm.

2.3.4 Preliminary Polymer Identification Scheme Based on Spectra from Nile Red-Stained Plastics

Preliminary analysis of the data reveals that groups of plastics stained with Nile Red exhibit distinguishable patterns when excited at different wavelengths. Emission peaks produced by 405 nm and 465 nm excitation wavelengths are most useful for polymer classification because all of the sample plastics emitted similar spectral peaks at 525 nm excitation. Using spectral data to distinguish between plastics and organic samples dyed with Nile Red is more complicated. At 405 nm and 525 nm excitation, organic materials and plastic materials share the same distinct spectral peaks. However, this is not the case at 465 nm. Therefore, there is a possible basis for plastic/organic differentiation by applying advanced spectral processing techniques such as deconvolution. This could be addressed in future work. A larger dataset and further measurements may also reveal other distinguishing factors for material differentiation models. Lastly, these peaks result from the specific excitation wavelengths and the long-pass filters. Prominent peaks may exist in the regions in between the excitation wavelength and long-pass filter cut-on wavelength.

Figure [2.8] depicts a basic polymer categorization scheme based on the spectral data from plastics stained with NR. This scheme has the potential to identify an unknown plastic polymer or identify it as a member of a specific group of plastics. Using Nile Red alone, it's difficult to distinguish between PP and PE, or between Nylon, PUR, and PVC. When excited by 465 nm and 525 nm, the spectral peaks of PVC are left of Nylon's and PUR's peaks which may aid in further categorization. However, given that the fluorescence spectra of stained plastics are a product of the polymer, additives, pigmentation, and fluorescent dye, a large range of polymer types needs to be rigorously tested to comprehensively capture the common additives and pigments present in consumer plastics found in the field.

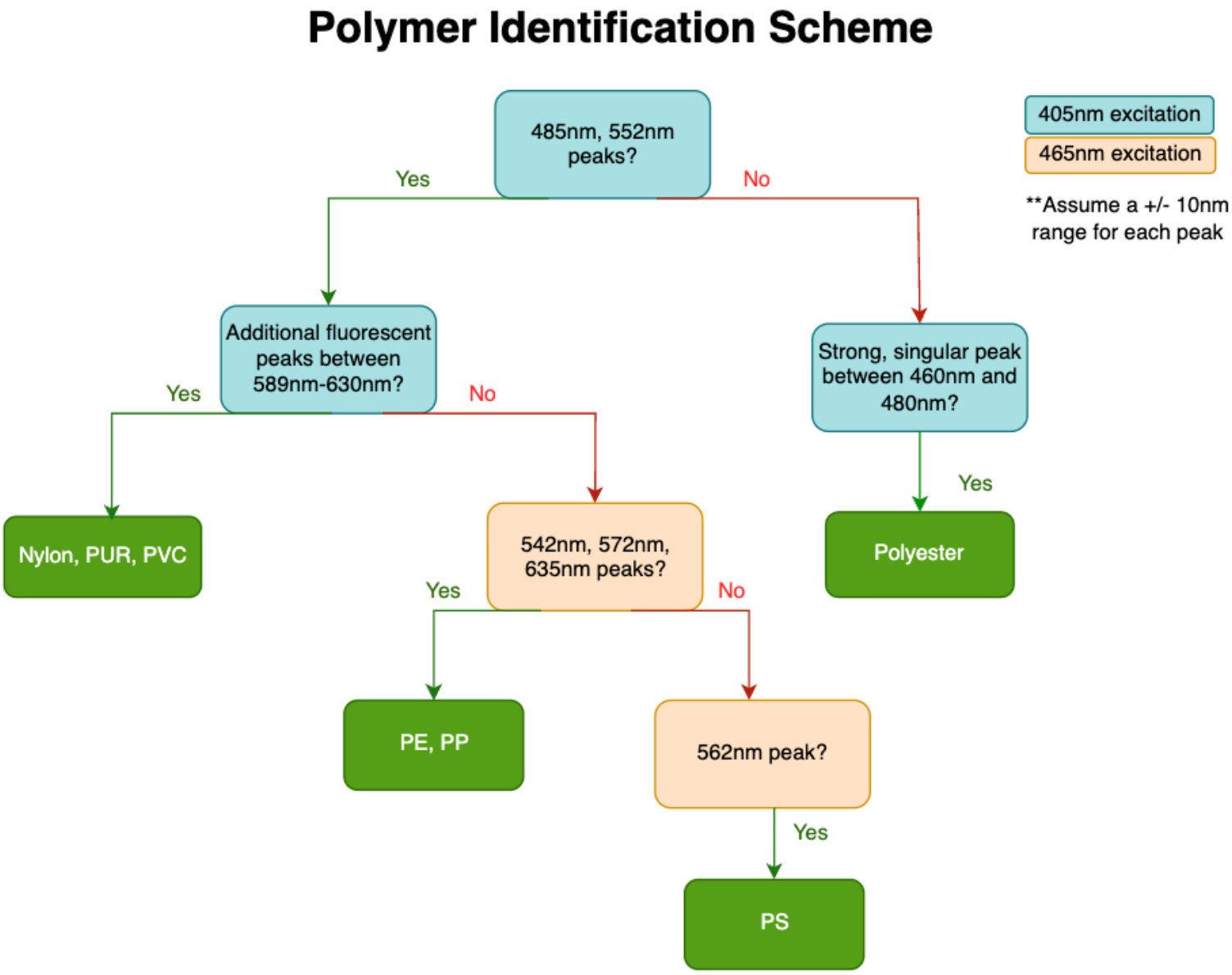

Figure 2.8: This polymer identification flowchart is based on the spectra collected from plastics stained with Nile Red. From the current dataset, it is difficult to find spectral characteristics that could further identify PE from PP and Nylon, PUR, and PVC from each other. Therefore, this process flow is conservative and intended as a preliminary interpretation of the spectral characteristics presented in this chapter. The next step is to encode and test this identification process within an automated tool that can extract and match spectral peaks to a standardized database.

2.3.5 Field Trials

Field trials were conducted to verify if plastics found in the natural environment could be matched and identified against the gathered spectral dataset. Plastics washed ashore along Magazine Beach in Cambridge, Massachusetts were collected and characterized using FTIR to verify chemical composition. Plastics whose polymer composition was successfully confirmed by FTIR were kept, leading to a dataset of 5 polypropylene (PP) samples and 3 polyethylene (PE) samples (see Appendix [A.8]-[A.15] for FTIR data). These samples were then characterized using the fluorimeter. Figure [2.9] presents the fluorescent emission spectral data for the excitation wavelengths of 405nm, 465nm, and 525nm.

The data from the field trials show that the preliminary polymer identification scheme displayed in Figure [2.8] could be used to correctly identify 80% of the polypropylene samples and 100% of the polyethylene plastics as either PE or PP in nature based on their spectral peaks alone. One polypropylene sample did not contain a prominent peak at 572 nm but contained the rest of the requisite peaks. Given that a plastic's spectral data is a function of the polymer, additives, pigments, and fluorescent dyes, a larger, diverse dataset will capture a more accurate spectral footprint for each polymer.

Furthermore, it's currently difficult to distinguish between polyethylene and polypropylene based on spectral data alone. Therefore, future work should investigate alternate pathways to distinguish between plastic polymers that share high similarities in fluorescent spectra.

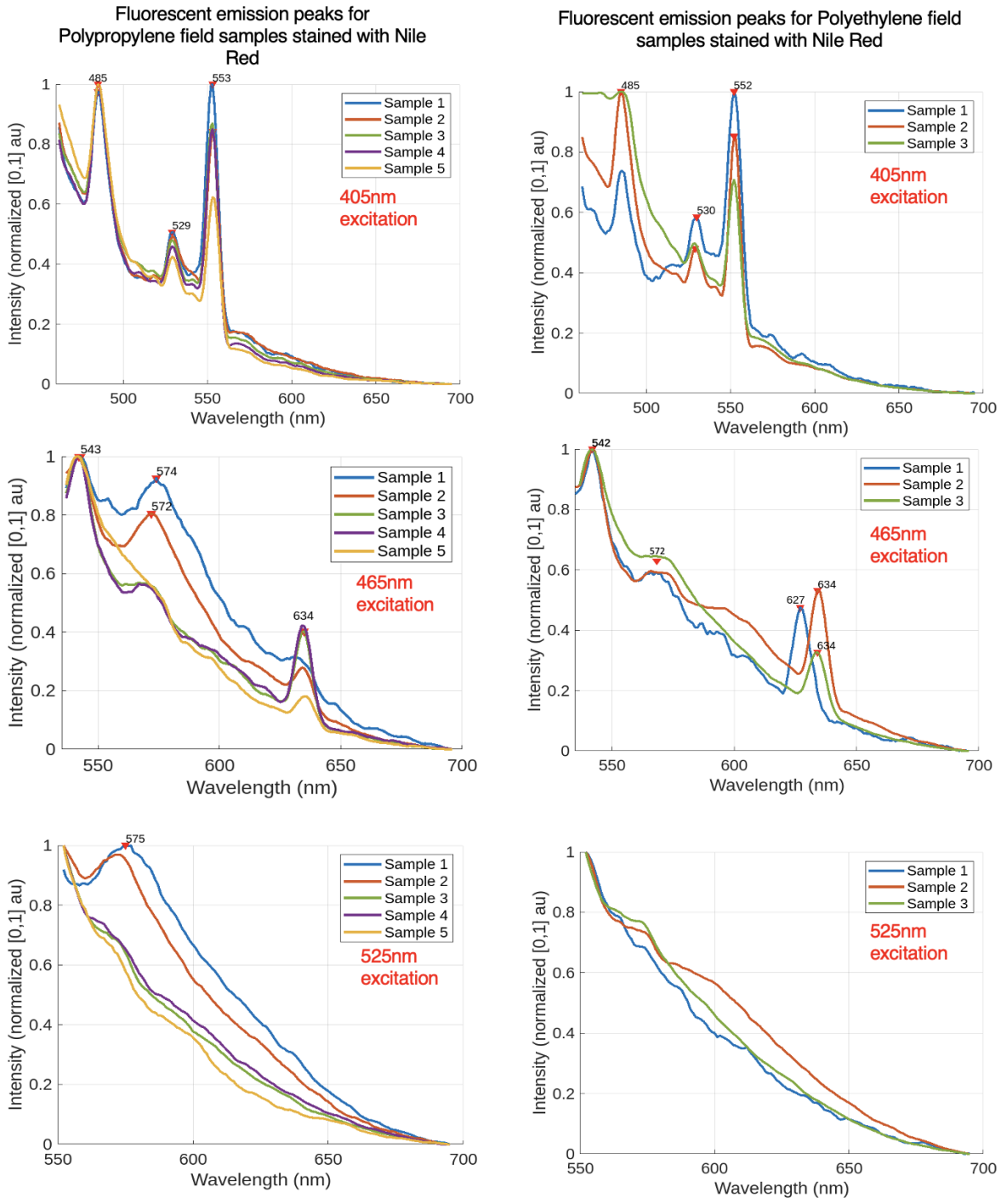

Figure 2.9: This graph displays the fluorescent spectra of 5 polypropylene field samples and 3 polyethylene samples for excitation at 405 nm, 465 nm, and 525 nm. Four polypropylene samples and all polyethylene samples share all spectral peaks for 405 nm and 465 nm excitation. For 525 nm excitation, the polyethylene samples contain no visible peaks, which indicates that the long-pass filter may have restricted the spectral window.

2.4 Summary, Conclusions, and Prognosis

The primary goal of this thesis is to collect data on Nile Red-based optical microplastic detection methods for future applications in portable, low-cost microplastic monitoring technology. This chapter presents preliminary fluorescent emission data of plastic and organic materials stained with Nile Red. By characterizing the fluorescent emission peaks for plastics stained with Nile Red, distinguishing spectral patterns can be observed.

The data showed that while using the spectra from plastics stained with Nile Red alone may offer some basis for distinguishing them from organic materials, it is not yet sufficient to be reliable due to spectral overlap at certain wavelengths. In these cases, high-resolution spectral characterization could offer the desired results.

The spectra also indicated the long-pass filters selected for this project may need to be refined. When excited at 525 nm, the cut-on filter at 570 nm often cut into the spectral window of polypropylene and polyethylene. Budget constraints limited the amount of long-pass filters purchased and the quantity of samples that could be processed by the fluorimeter. In the future, the long-pass filters should be refined to maximize spectral windows. Using a laser for excitation rather than a Xenon lamp will also decrease wayward noise from the excitation fluorescence.

While this was a preliminary study, future work should focus on collecting and characterizing a larger dataset of plastics to account for the inevitable variance introduced by plastics with different pigments, additives, and surface conditions. Weathered plastics found in the field consisting of polymers other than polyethylene and polypropylene should also be tested. A comprehensive dataset may be used to train a model to categorize plastics based on fluorescence spectra alone. The polymer identification scheme displayed in Figure [2.8] can then be encoded into an automated tool. While some studies [17], [23], [24], [26] have conducted preliminary research on using photoluminescence for microplastic characterization with and without fluorescent dyes, a robust model has yet to be fully developed.

Chapter 3

Pairing spectral data with a low-cost microplastic imaging configuration for rapid polymer identification

Chapter 2 introduced spectral datasets of plastic and organic samples stained with Nile Red. The chapter discussion highlighted normalized spectral peaks for specific materials and proposed a preliminary identification scheme based on the data. This chapter will present photographs of stained plastic and organic samples taken with a Raspberry Pi camera and illuminated using commercial LEDs with similar excitation wavelengths from the previous chapter. The photographs will then be compared with the raw spectral data to qualitatively demonstrate how the spectral dataset can inform a low-cost fluorescent imaging method for microplastic detection.

3.1 Motivation

Nile Red is a solvatochromatic dye, which means that its emission color will shift based on the polarity of a polymer. Other factors influencing the color shifts are plastic consumer additives, pigments, and the Nile Red solvent. Maes et al. (2017) suggested that Nile

Red's solvatochromic nature could be used to distinguish between polymers. Several studies have proposed other imaging methodologies and analyses for Nile Red-stained microplastic quantification. Sturm et al. (2023) and Meyers et al. (2022) have presented research successfully demonstrating automated identification processes for microplastics stained with Nile Red using fluorescent imaging and image analysis [8], [9]. However, these studies have been conducted using images taken with a fluorescent microscope, which can be costly and not easily accessible in the field. This chapter aims to demonstrate a proof-of-concept that an automated microplastic detection program could be developed for a lower cost on field-portable instrumentation based on images taken using a Raspberry Pi-based fluorescence imaging system and data presented in Chapter 2.

3.2 Imaging Methods

3.2.1 Fluorescence Imaging System Set-Up and Image Collection

An imaging system (Figure [3.1]) was specially designed and manufactured to illuminate and image the stained samples. The system primarily consists of a Raspberry Pi (RPi) Model 4B and a 64-megapixel Arducam Hawkeye camera capable of autofocus. Images were captured using the libcamera library. The same long-pass filters used in Chapter 2 were used in this system to block excitation light from entering the camera lens. The system possessed a slot below the camera to mount the long-pass filter. UV, blue, and green LEDs used for excitation were attached just underneath the filter. The wavelengths of the LEDs were 405 nm, 465-470 nm, and 525-530 nm, based on the provided manufacturer's data. Two sets of LEDs, UV and RGB, were attached to the RPi, which could easily switch between the different LED sets. Including the long-pass optical filters, the system cost under $450 to build. Without the long-pass optical filters, the system cost under $200 to build. Future iterations can explore low-cost filters such as Roscolux gels instead of the Schott glass filters to reduce cost further.

Imaging was conducted in a dark room to increase the quality of images and reduce optical interference. The images presented in this chapter are fragments from samples used for spectral data collection in Chapter 2. The visual appearance of these samples was then compared to their spectral data. For details on sample composition and the staining process, see Chapter 2, Section 2.2.

The NR-stained plastic samples that were characterized by the fluorimeter in Chapter 2 were reused for this study. The same samples were cut into smaller fragments < 5 mm for imaging. The stained samples were placed on the stage and illuminated using LEDs. Three images were taken for an excitation wavelength of 405 nm, one for each long-pass filter with cut-on wavelengths of 455 nm, 530 nm, and 570 nm. Two images were taken for an excitation wavelength of 465 nm, one each with a 530nm and 570 nm long pass filter. Only one image was taken for an excitation wavelength of 525 nm using the 570 nm long pass filter. A final image was also taken of the samples with white light illumination and no filters. A total of seven images were taken. Afterwards, the images were saved by the Raspberry Pi in .jpg format and were not altered before being presented in this Chapter.

At a plastic's highest emission intensity peak for a given wavelength and optical filter, it's expected that the microplastic will also visually be the brightest for the same wavelength and filter combination. Similarly, the plastic is expected to be the least bright at the lowest emission intensity peak for the same wavelength and filter combination. Quantifying visual differences in fluorescent intensities and the color of plastics excited at different wavelengths may provide rapid, critical cues to distinguish between polymers.

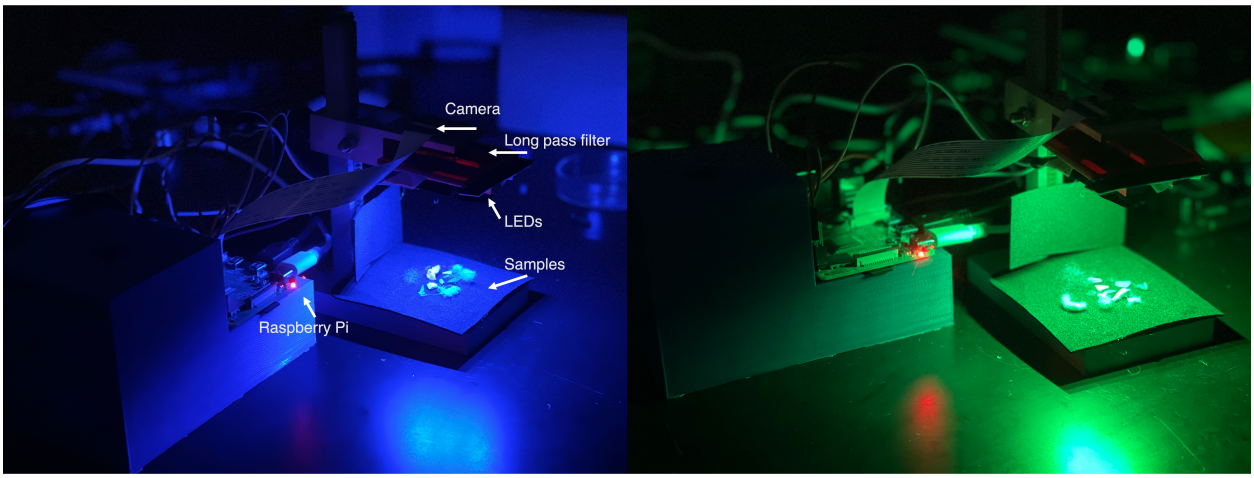

Figure 3.1: The system excites a sample with blue light (left) and green light (right). An adjustable mount allows the user to raise and lower the camera to adjust focus. A long pass filter with a 570 nm cut-on wavelength can be seen fixtured below the camera.

3.3 Results and Discussion

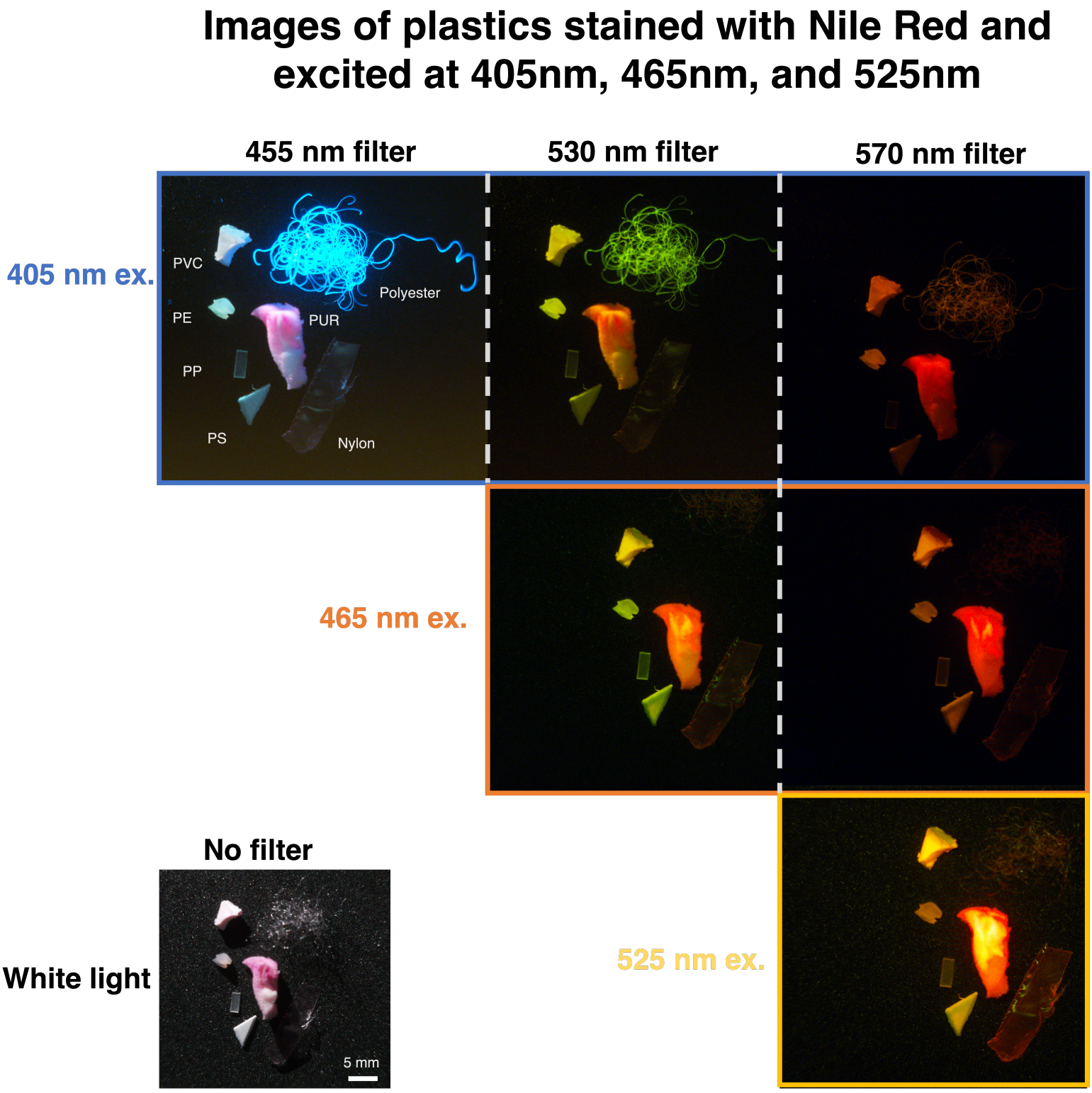

Figure 3.2: Fragments from seven plastics stained with Nile Red are depicted. Similar to the spectral data recorded in Chapter 2 for NR-stained plastics, the strongest fluorescent intensity for several plastics is elicited by a 525 nm excitation wavelength with a 570 nm cut-on filter or 405 nm (in the case of Polyester's strong autofluorescence) with a 455 nm cut-on filter. The weakest excitation wavelength and filter combination appears to be 405 nm excitation with a 570 nm cut-on filter.

3.3.1 Nile Red Stained Plastic Samples

Figure [3.2] shows fragments of plastics stained with Nile Red. The plastics exhibit noticeably various colors and fluorescent intensities at different wavelengths. The images can be encoded into a trainable dataset for rapid polymer identification analysis. To examine how each plastic visually fluoresces compared to its recorded spectra, Figures [3.3] to [3.9] each juxtapose the image of a Nile Red-stained plastic sample from Figure [3.2] against its graphed spectral data when excited at 405 nm, 465 nm, and 525 nm.

Figure [3.3] displays the spectra and microplastic images of Nile Red-stained polyethylene. When excited with 405 nm and using a 455 nm long pass filter, PE will be pale blue with a high fluorescent intensity. If the filter is changed for a 530 nm long pass filter, PE will appear green-yellow but with little drop in fluorescence intensity. If the excitation wavelength changes to 465 nm but the 530 nm long pass filter is kept, then PE appears to dim slightly. If a 570 nm long pass filter is used, PE will be yellow-orange and may appear dimmer compared to 405 nm excitation.

Figure [3.4] displays the spectra and microplastic images of Nile Red-stained polystyrene. When excited with 405 nm and using a 455 nm long pass filter, PE will be turquoise blue and somewhat dim. If the excitation wavelength is changed to 465 nm with a 530 nm long pass filter, then PS will appear green-yellow but with little drop in fluorescence intensity. If the excitation wavelength changes to 525 nm with a 570 nm long pass filter, PS will adopt the brightest intensity.

Figure [3.5] displays the spectra and microplastic images of Nile Red-stained polypropylene. When excited with 405 nm and using a 455 nm long pass filter, PE will be pale blue and the dimmest of the three excitation wavelengths. If excited by 465 nm with a 530 nm long pass filter, PP will appear green. If the filter is changed for a 570 nm long pass filter with 525 nm excitation, PP will be yellow, and potentially equally fluorescent.

Figure [3.6] displays the spectra and microplastic images of Nile Red-stained nylon. When

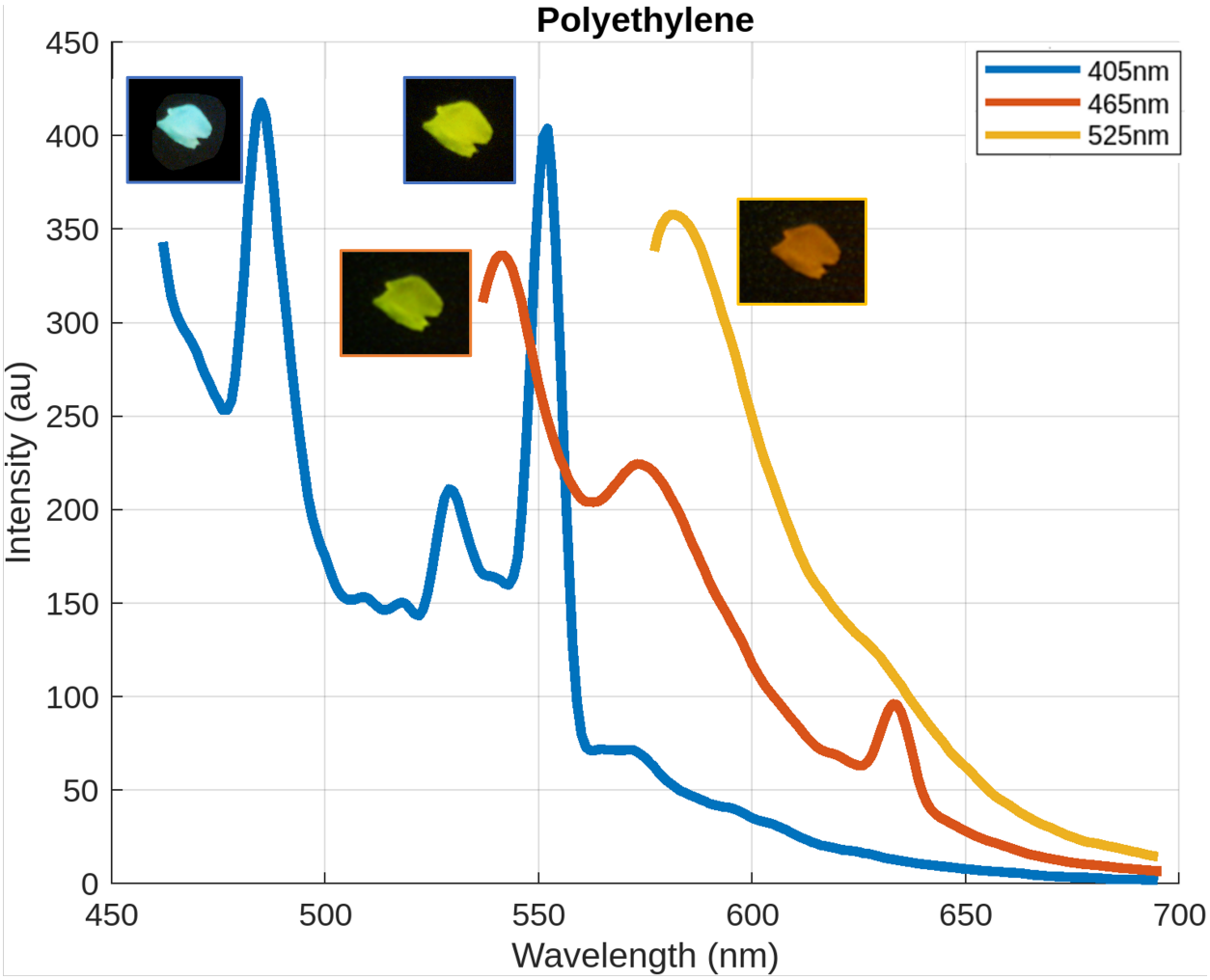

Figure 3.3: Nile Red-stained polyethylene is excited at wavelengths 405 nm, 465 nm, and 525 nm. PE experiences its two strongest emission intensities when excited by 405nm. Correspondingly, the two brightest images of PE in Figure [3.2] were both taken using the 405nm excitation wavelength (one image used the 455 nm filter and the other 530 nm). These cropped images are visibly brighter than those depicting PE excited by either 465 nm or 525 nm excitation wavelengths.

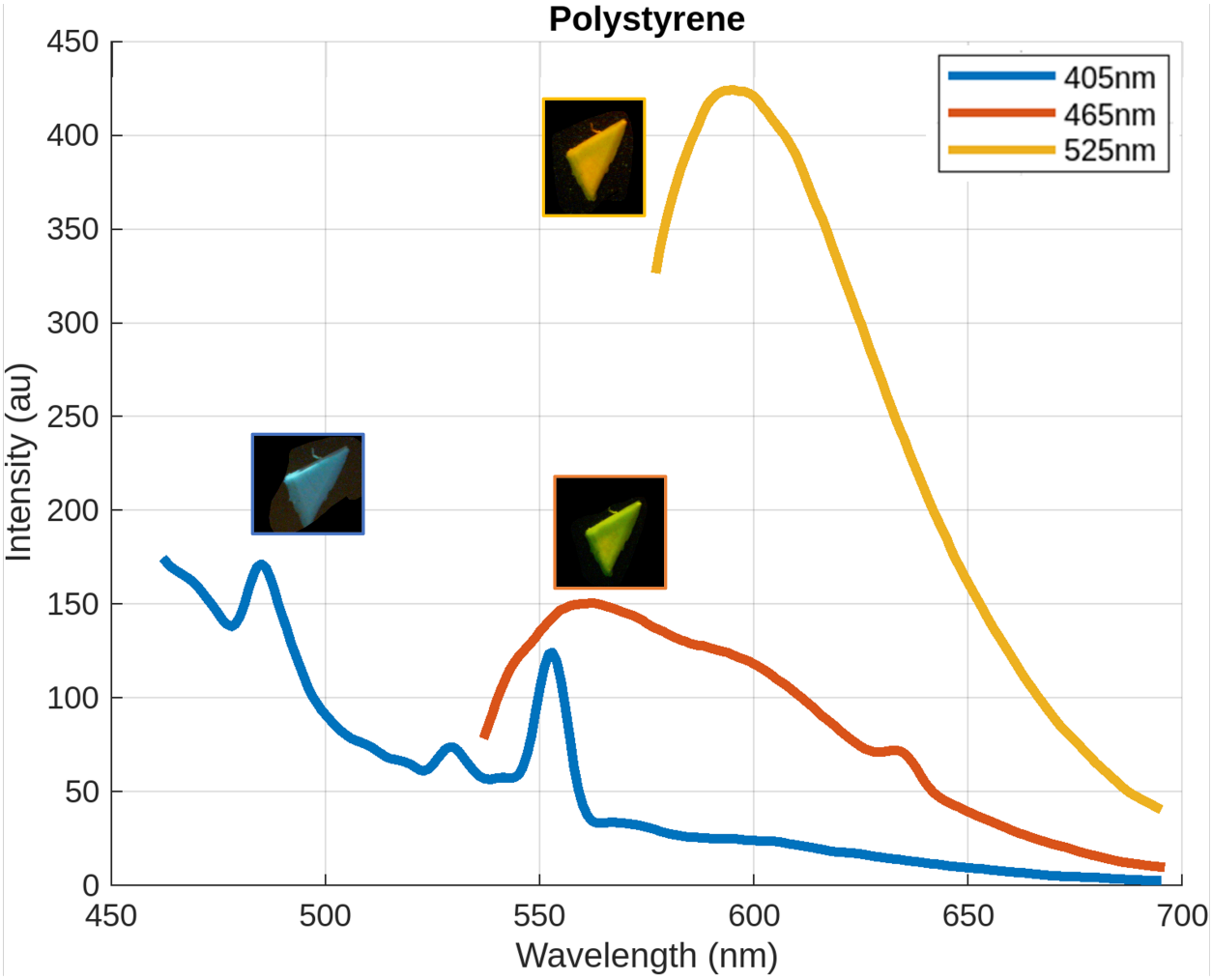

Figure 3.4: Nile Red-stained polystyrene is excited at wavelengths 405 nm, 465 nm, and 525 nm. PS appears the brightest when using a 525 nm excitation wavelength and 570 nm filter. This fits well with the spectra data given that the peak emission intensity is approximately 590 nm with a 525 nm excitation.

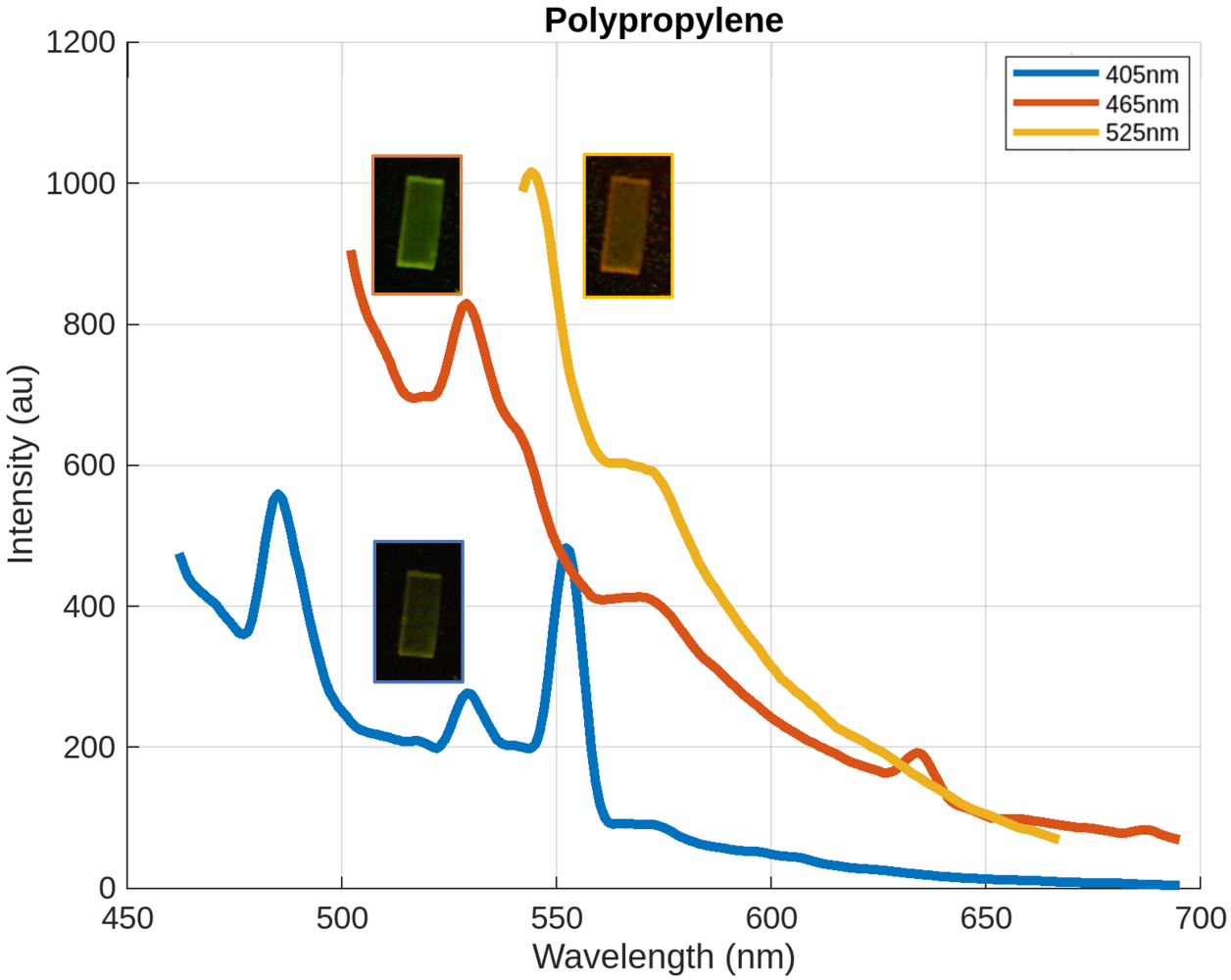

Figure 3.5: Nile Red-stained polypropylene when excited at wavelengths 405 nm, 465 nm, and 525 nm. Visually, the peaks excited by 465 nm and 525 nm seem equally bright, and their spectral peaks are similarly close. The peak excited by 405 nm is noticeably dimmer, both visually and graphically.

excited with 405 nm and using a 455 nm long pass filter, nylon will be pale blue with a low fluorescent intensity. If the filter is changed for a 530 nm long pass filter, nylon will appear pale green but with even less fluorescence intensity. If the excitation wavelength changes to 465 nm with the 570 nm long pass filter, then nylon might appear slightly more fluoresent with a red tinge. If a 570 nm long pass filter is used with 525 nm excitation, nylon will be red and the most fluorescent of all three excitation wavelengths.

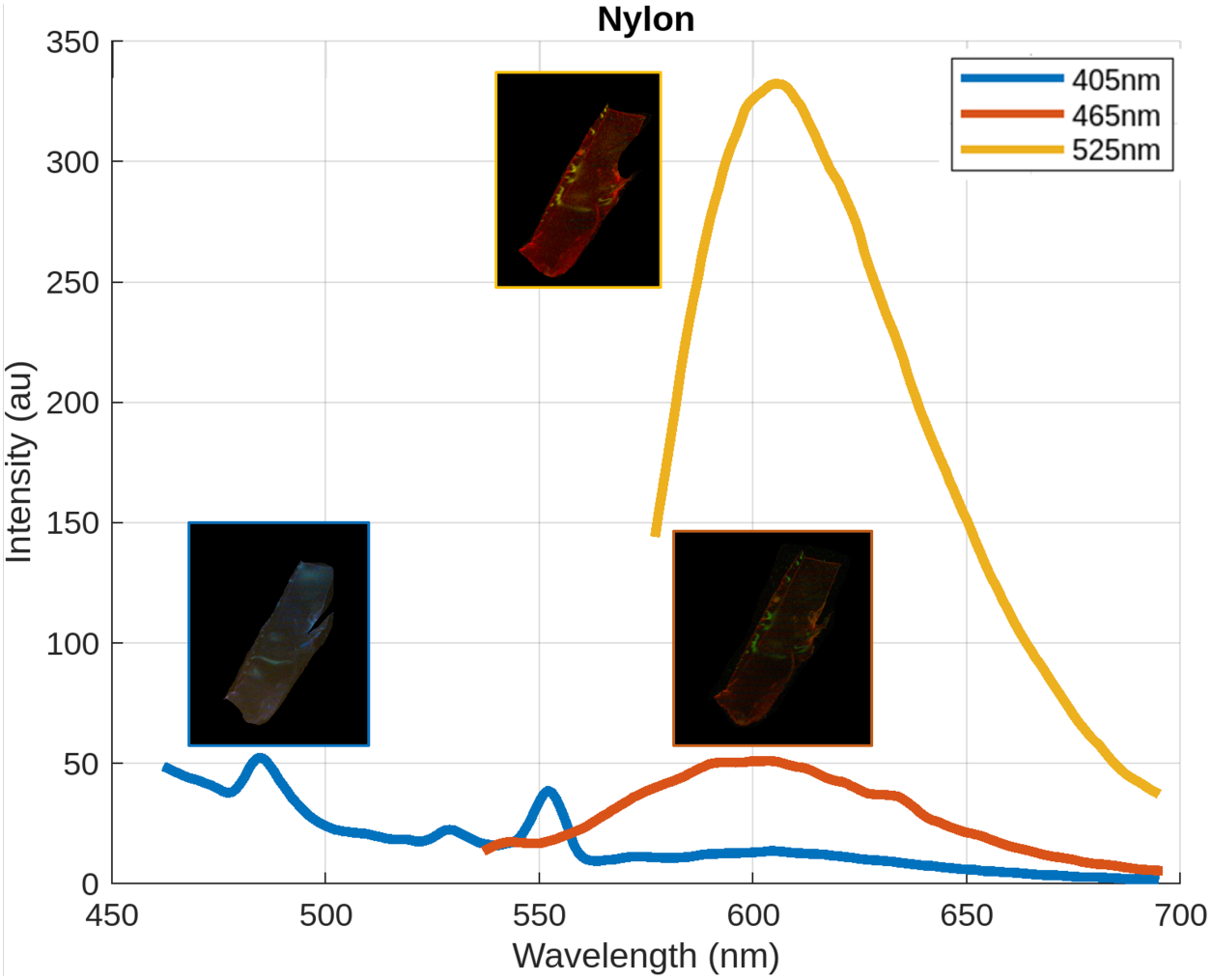

Figure 3.6: Nile Red-stained nylon is excited at wavelengths 405 nm, 465 nm, and 525 nm. Visually, nylon is the brightest when excited at 525 nm and photographed through the 570 nm filter. This aligns well graphically, where Nylon's highest emission peak is located near 610 nm with an excitation wavelength of 525 nm. The dimmed appearances of Nylon excited by 405 nm and 465 nm in comparison to 525 nm match the graphed spectra.

Figure [3.7] displays the spectra and microplastic images of Nile Red-stained polyester.

Polyester will only appear blue when excited with 405 nm and using a 455 nm long pass filter, but will otherwise be quite dim for other excitation wavelengths.

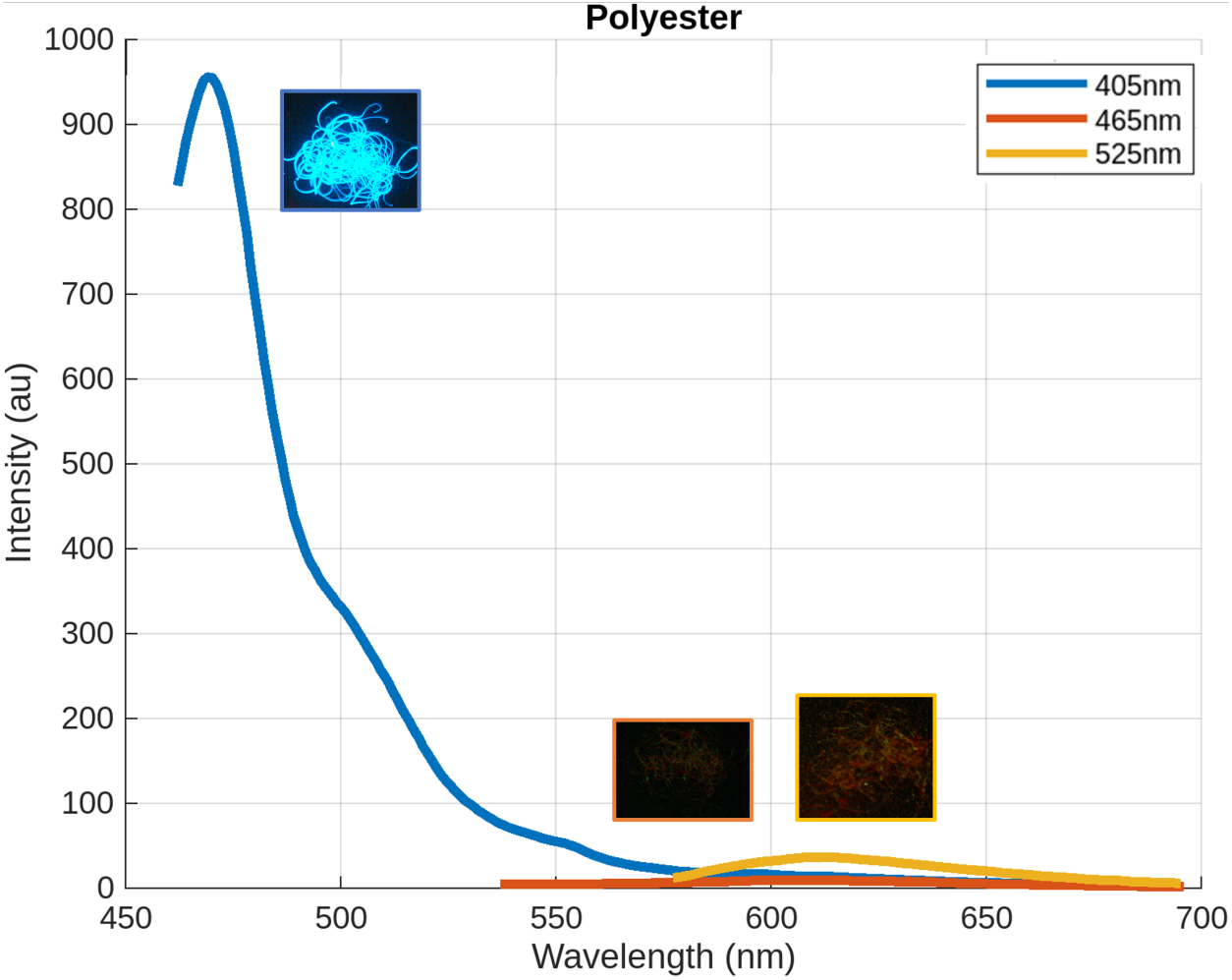

Figure 3.7: Nile Red-stained polyester is excited at wavelengths 405 nm, 465 nm, and 525 nm. From the images, Polyester is strongly fluorescent when excited by 405 nm and seen through a 455 filter. When excited by 525 nm, red-tinted Polyester can be faintly seen, while little to no fluorescence can be seen at all for 465 nm excitation. These results match the graphed relative intensity peaks.

Figure [3.8] displays the spectra and microplastic images of Nile Red-stained polyurethane. When excited with 405 nm and using a 455 nm long pass filter, PUR will be possess low fluorescent intensity and may appear blue. If the filter is changed for a 570 nm long pass filter with a 465 nm excitation wavelength, the PUR will appear orange and more fluorescent than PUR illuminated by 405 nm. If excited by 525 nm with a 570 nm long pass filter then

PUR will appear intensely bright and red.

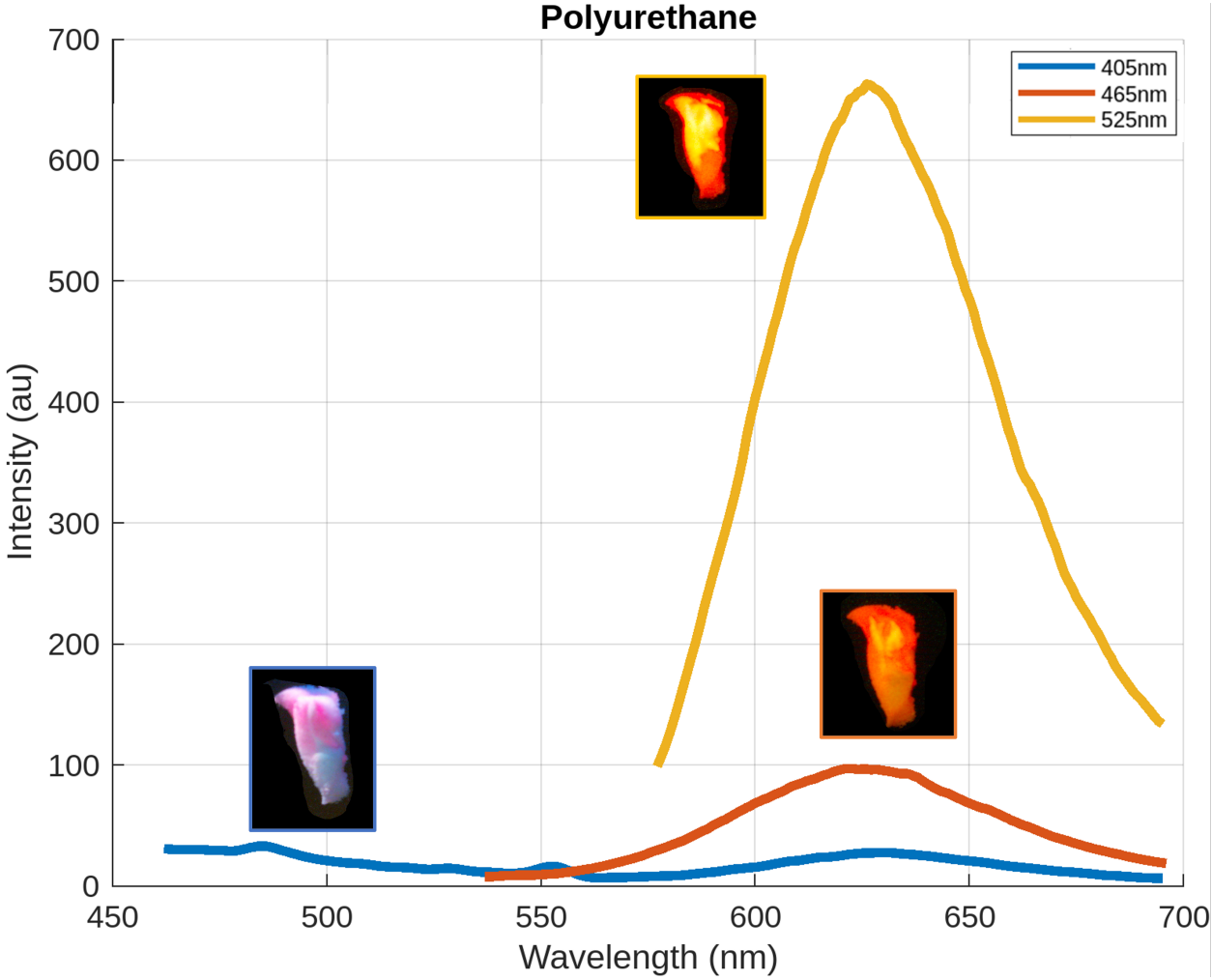

Figure 3.8: Nile Red-stained polyurethane is excited at wavelengths 405 nm, 465 nm, and 525 nm. The cropped images from Figure [3.2] are visually brightest at 525 nm excitation, and progressively less bright at 465 nm and 405 nm excitation, respectively. These visual characteristics match the highest spectral emission intensity peak at approximately 625 nm when excited by 525 nm.

Figure [3.9] displays the spectra and microplastic images of Nile Red-stained polyvinyl chloride. When excited with 405 nm and using a 455 nm long pass filter, PVC will be pale blue with a lower fluorescent intensity. If the excitation wavelength changes to 465 nm but the 530 nm long pass filter is kept, then PE appears to dim slightly. If a 570 nm long pass filter is used, PE will be significantly yellow-orange and may appear dimmer.

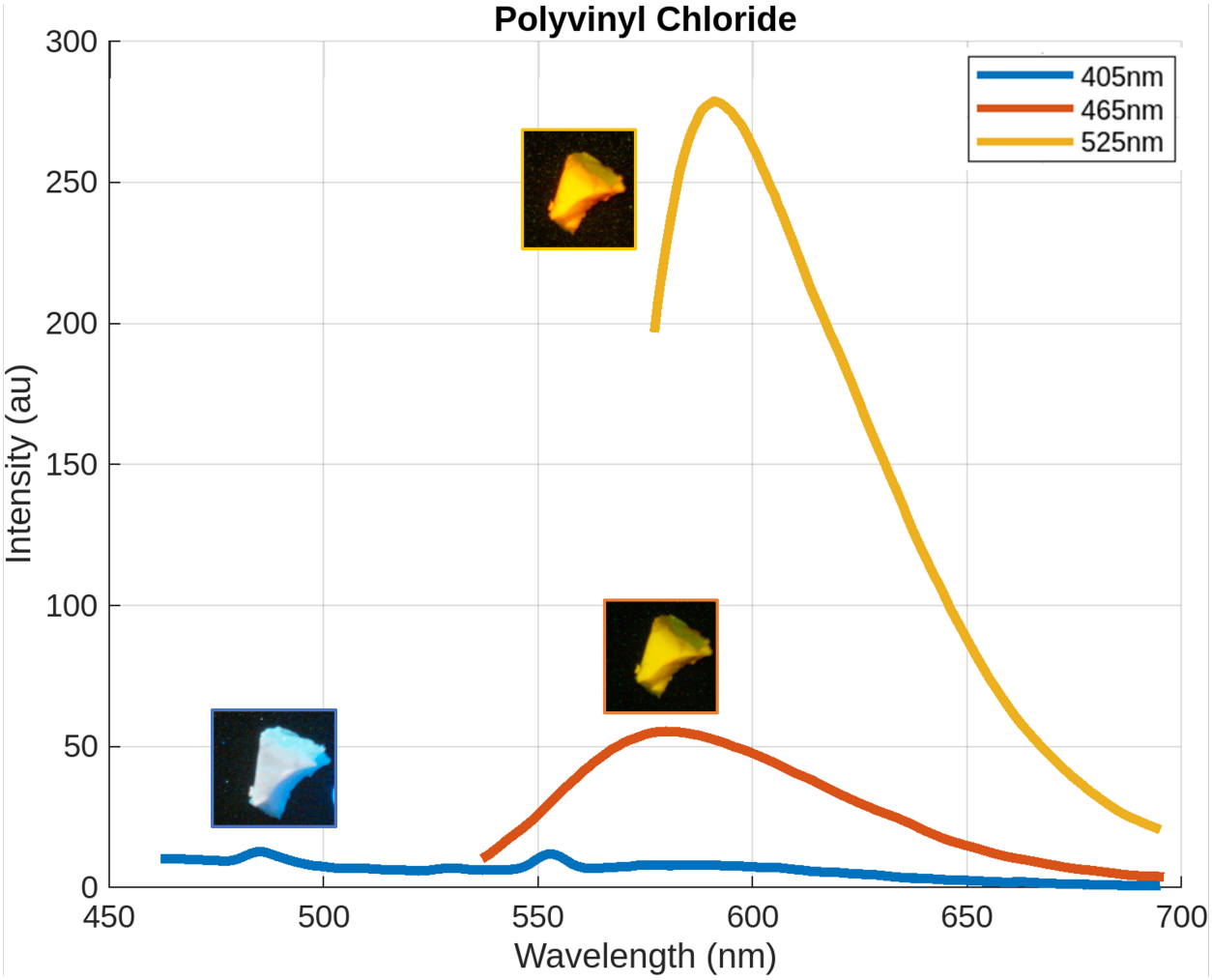

Figure 3.9: Nile Red-stained polyvinyl chloride is excited at wavelengths 405 nm, 465 nm, and 525 nm. PVC is visually brightest with a 525 nm excitation, similar to the highest emission intensity peak at 525 nm within the spectra.

3.4 Conclusion and Future Work

Each sample's relative spectral fluorescent intensity peaks were compared with the relative visual brightness of the sample's image at each peak. For each plastic, the sample image closely matched the spectral characteristics. The results qualitatively validated that the spectral data can predict the visual relative fluorescence intensity and color shift of microplastic images taken for a given wavelength and filter combination.

This dataset is preliminary proof that rapid polymer identification can be achieved by imaging plastics with a series of different excitation lengths and optical filters. Future work should investigate leveraging image analysis software to create a model that can identify polymer types based on this system's images. This low-cost setup could be adapted to perform rapid, real-time plastic analysis in the field.

Chapter 4

Utilizing low-cost photodiodes for microplastic detection in liquid samples

The work in this chapter was presented at the 2023 IEEE OCEANS Limerick conference and published in the conference proceedings (Prasad et. al, 2023) [27] [1]. The work was reformatted and reproduced here.

Chapters 2 and 3 present an optical microplastic detection premise based on imaging dried, stained microplastic samples. However, in situ microplastic detection is more suited to field deployments and ocean-going applications and reduces labor and laboratory instrument costs. Therefore, this chapter presents a proof-of-concept of an inexpensive optical detection system developed to quantify the presence of microplastics within liquid samples.

4.1 Motivation

Given that water cannot be a solvent for Nile Red, most Nile Red-based fluorescent microplastic detection schemes include filtering and drying of samples due to the difficulties

[1] © 2023 IEEE. Personal use of this material is permitted. Permission from IEEE must be obtained for all other uses, in any current or future media, including reprinting/republishing this material for advertising or promotional purposes, creating new collective works, for resale or redistribution to servers or lists, or reuse of any copyrighted component of this work in other works.

posed by in situ sampling. These include but are not limited to the increased false positives caused by the development of dye aggregates and lower microplastic fluorescence within in situ samples [10]. However, in situ sampling methods would remove the laborious process of filtration and dying samples and would increase the capacity for rapid analysis in the field. Given this motivation, larger microplastics such as virgin plastic pellets, or nurdles, were established as the optimal microplastic target for the system. Nurdles, which range in size from approximately 1mm to 5mm, are used as raw material in plastic extrusion and injection molding processes for the production of everyday plastic items and span a range of plastics such as polyethylene, polypropylene, polystyrene, and polyvinyl chloride. However, inadequate waste management and large-scale container ship spills have led to the annual release of millions of nurdles into the environment, and they are estimated to be the second largest source of microplastic pollution in the ocean [28]. Due to their small size, these plastic fragments have propagated throughout marine and terrestrial ecosystems. Nurdles are commonly found washed up on beaches and in the digestive tracts of marine animals that have mistaken them for food. Nurdles were chosen as the target partially due to their significant threat to marine wildlife, but also due to their size and surface condition. Larger microplastics will not be mistaken for dye aggregates and will likely emit higher levels of fluorescence that make detection easier. Furthermore, virgin plastics are typically clear, translucent, or white, which are favorable physical characteristics for emitting high fluorescence when stained with Nile Red [29], [30].

The design considerations for the system were simplicity, low-cost, rapid analysis, and portability. The proposed system uses a silicon photodiode and a light-focusing lens to detect fluorescent microplastics (MPs) stained by Nile Red. Signal outputs were amplified and recorded on a Raspberry Pi 4 with the aid of an analog voltage measurement attachment. Preliminary results were obtained for laboratory-created test solutions containing NR-stained MPs of known type, quantity, and dimension. These results showed the system output was linear with MP concentration of the test solutions. Future work should focus on validating

the system with field samples and incorporating a polymer identification scheme into the system.

4.2 Materials and Methods

4.2.1 Chemicals

This study used translucent polypropylene (PP) pellets. These are among the most common type and form factor of microplastics found in the environment. These plastics are low-density and float on the water surface. The pellets were roughly 3x3mm^2 and were hand-cut into sample sizes ranging from 0.5x0.5mm^2 to 3x3mm^2. A commercially available 10 µg/mL acetone Nile Red (NR) solution was procured for this experiment. All solutions and suspensions were prepared with Milli-Q water.

Nile Red-stained microplastics made of polypropylene have an excitation wavelength in the range of 450 - 490 nm and a corresponding emission wavelength in the range of 515-590 nm [6]. Component selection for the optical detection system were tailored to these characteristics.

The fluorescence detection scheme relied on an FDS010 silicon photodiode purchased from Thorlabs. The silicon photodiode was chosen primarily due to the proximity of its responsivity peak to NR's emission peak at the given price point. The photodiode converts optical power to electrical current, which can be converted to an output voltage by placing a load resistor (R_L) between the photodiode anode and the circuit ground. The output voltage can be calculated as

$$Vo = P + R(\lambda) + R_L \tag{4.1}$$

Where P is the optical power (the fluorescent emissions in this case) and R(λ) is the responsivity (A/W) which is dependent on the wavelength of the fluorescent light. Figure

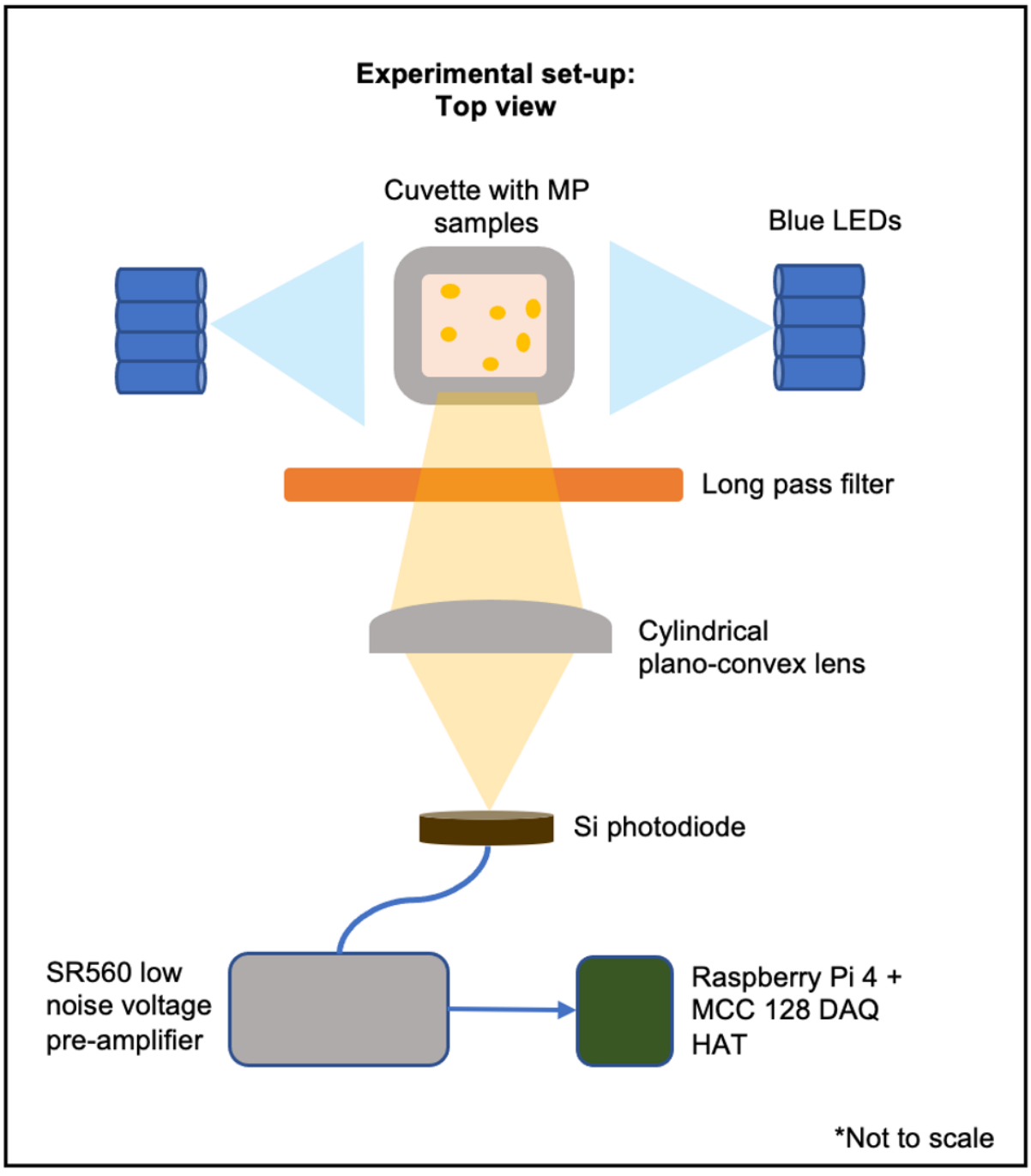

Figure 4.1: This figure presents a top view of the experimental set-up (not drawn to scale). Blue light from the LEDs excites the microplastics in the cuvette, causing them to fluoresce. Fluorescing light passes through the long pass filter (which eliminates the blue LED light) and is then focused by the plano-convex lens into the photodiode receptor.

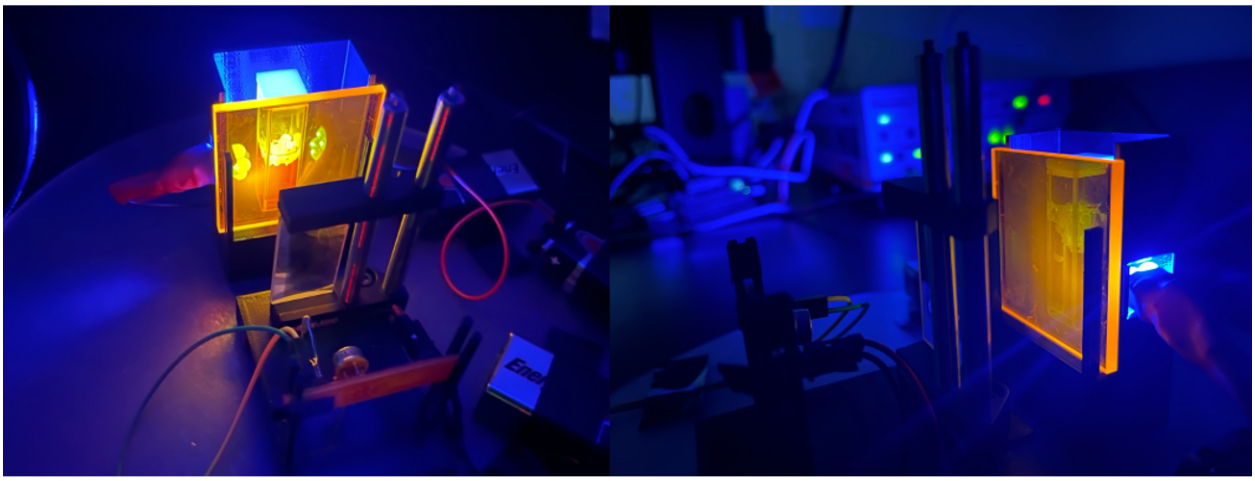

Figure 4.2: This figure presents images taken of the experimental set-up. A custom rig was 3D printed to hold and position the system components.

4.3 shows the circuit diagram of the optical detection system. An RC circuit was also implemented to filter noise.

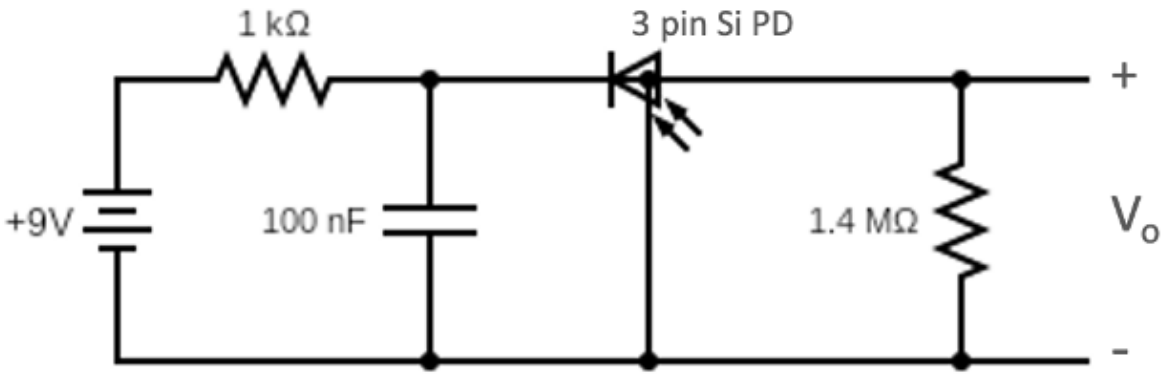

Figure 4.3: This figure presents the circuit schematic used in the optical detection system. An RC configuration acts as a noise filter. A large value was chosen for R_L based on Equation 1.

Eight blue light-emitting diodes (LEDs) were chosen to excite the MPs in NR due to cost and ease of access. These LEDs are commonly available components with an emission wavelength of 465 nm. A long-pass filter with a cut-on of 530 nm was used to filter the blue excitation light from the photodiode and ensure only emission wavelengths were detected. A Thorlabs LJ1125L2-A cylindrical plano-convex lens was then used to focus the excitation

light on the photodiode. This lens is capable of focusing parallel light rays into a single line, which is determined by the focal length of the lens. A Raspberry Pi 4 combined with an MCC 128 analog voltage measurement device was used to record output signals from the optical detection system. The MCC 128 provided a 16-bit analog input resolution and a maximum sample rate of 100 kS/s. Photodiodes produce low-amplitude currents and therefore signals are commonly amplified with a transimpedance amplifier or a pre-amplifier after the current has been converted to a voltage. For each quantity of MPs in a given solution, raw output signals were amplified 10x and 100x using an SR560 low noise voltage pre-amplifier.

4.2.2 Experimental Procedure

Various volumes of the 10 ug/mL NR stock solution were diluted with Milli-Q water to create NR solutions with concentrations of 1 ug/mL, 2 ug/mL, and 3 ug/mL. Each solution concentration was tested with five different quantities of added MPs (0.1g, 0.2g, 0.3g, 0.4g, 0.5g). This resulted in MP solution concentrations of 0.04 g/mL, 0.08 g/mL, 0.12 g/mL, 0.16 g/mL, and 0.20 g/mL. Studies on MP concentrations in the environment vary by region and are not standardized. This system is also designed to operate in environments with higher-density MPs, such as coastal regions or regions near plastic spillages. For example, the system was initially designed to detect the presence of pellets in the water, not microfibers. Therefore, the MP concentrations in this study were chosen such that the change in fluorescence from each sample concentration would be visually noticeable and could be correlated with the presence of larger MP fragments, such as nurdles.

Initially, an optically clear square cuvette was filled with 2.5 mL of 1 ug/mL Nile Red solution. 0.1g of MPs were then added to the cuvette to create a 0.04 g/mL MP solution. Given the low density of the MPs, the cuvette was gently shaken to allow the solution to fully coat the injected MPs. After thirty minutes, the solution was irradiated with blue light and the output signal was amplified and then recorded using the Raspberry Pi 4. For each sample injected with MPs, 100 output voltage readings were recorded 0.5 seconds apart

and averaged together. This was done for each amplification level (unamplified output, 10x amplification, and 100x amplification) for every sample tested. The experiment was then repeated for different MP concentrations (0.08 g/mL, 0.12 g/mL, 0.16 g/mL, 0.20 g/mL) and for each remaining prepared concentration of NR solution (2 ug/mL and 3 ug/mL NR solutions).

The wait time between MP injection and signal recording was intentionally chosen based on literature that showed the fluorescent intensity of plastics stained with Nile Red to increase up to thirty minutes after initial dye injection, and then plateau between thirty to sixty minutes. Current studies show that organic material takes longer to stain with NR than plastics [6]. Therefore, a time frame that optimizes both low duration and high fluorescence enables rapid testing and prevents false positives resulting from stained organic material.

4.3 Results and Discussion

Figures 4.4 through 4.6 show the signal output corresponding to polypropylene quantity in prepared Nile Red solutions ranging from the control solution of 0 µg/mL to an NR concentration of 3 µg/mL. Figure 4.7 shows images of the prepared samples.

The preliminary data indicates that the signal output increases linearly for known linear increases in MP sample quantities. The average signal output also increases with higher Nile Red solution concentration.

Generally, data from each NR solution had R^2 values greater than 0.9. However, the system seemed to have the highest R^2 values using the 3 µg/mL NR solutions. This is likely due to the stronger fluorescence from the increased amount of dye. The slopes of the trend lines also do not vary significantly between unamplified data and 100x amplified data. This provides evidence that an external amplifier may not be needed in the system if noise can be effectively filtered by circuit components alone.

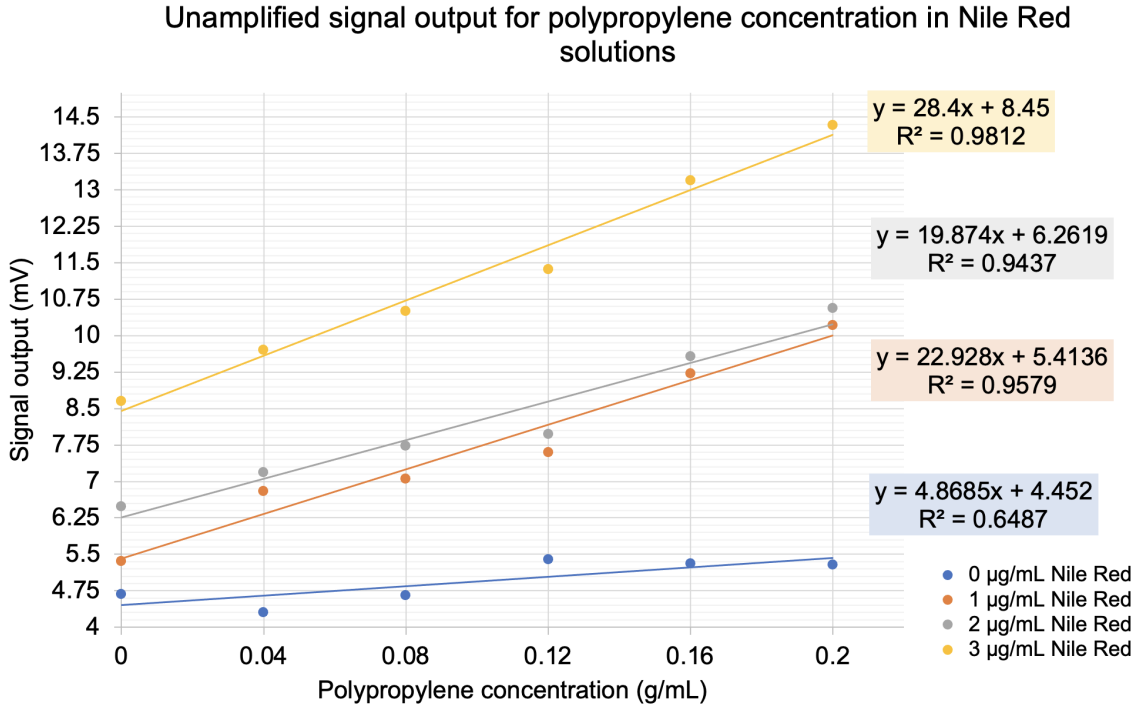

Figure 4.4: Unamplified signal output in mV versus microplastic concentration. Each data series represents a different solution concentration of Nile Red. Trend lines show a strong linear fit for the unamplified data.

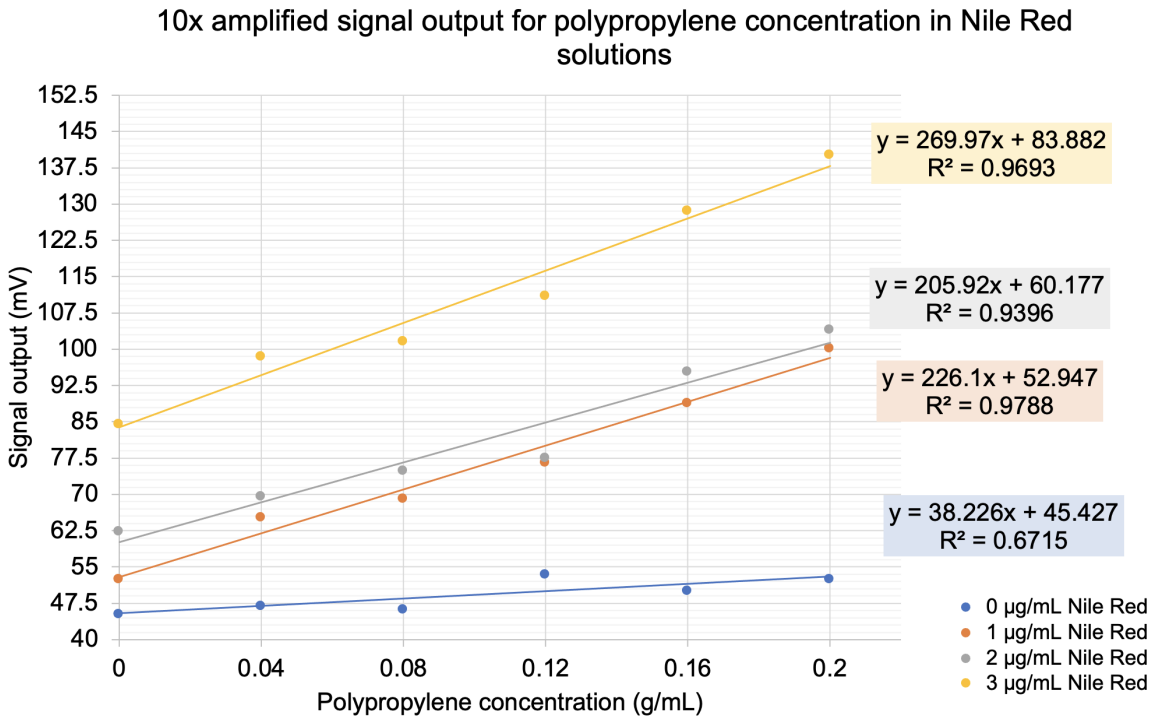

Figure 4.5: This figure presents 10x amplified signal output in mV versus microplastic concentration. Each data series represents a different solution concentration of Nile Red. Compared to the unamplified data, 10x amplification still provides a linear fit with minimal introduction of noise.

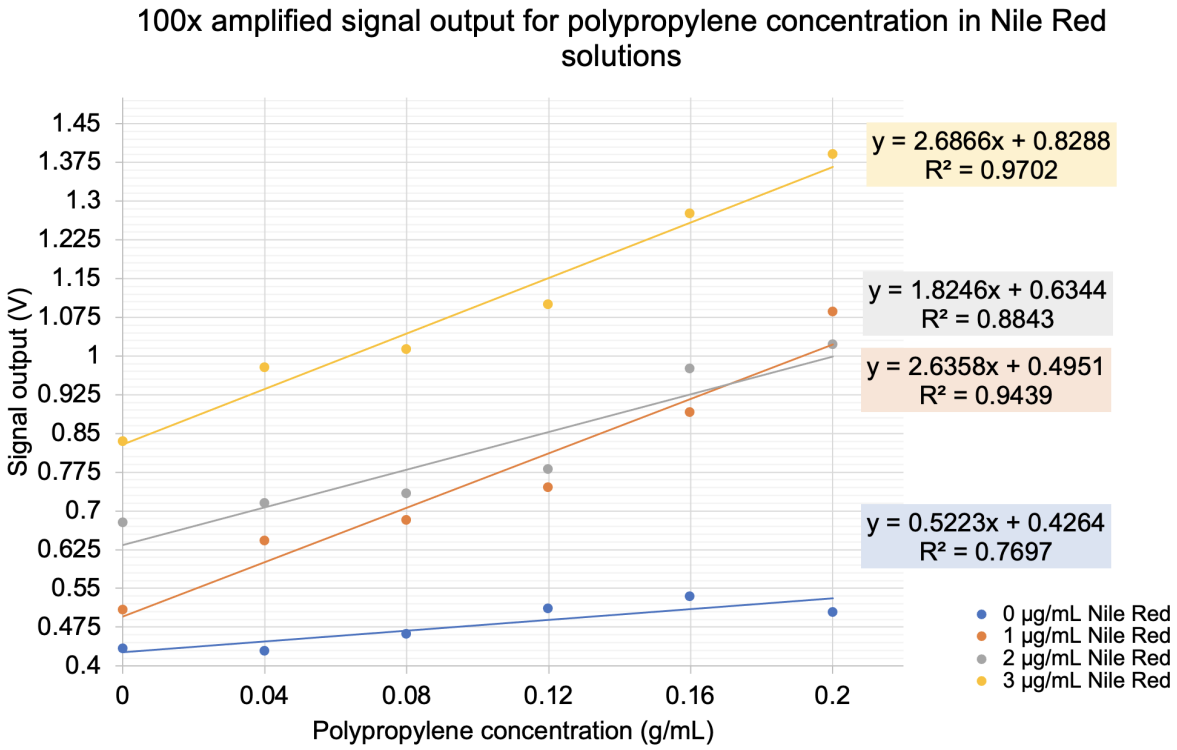

Figure 4.6: This figure presents a 100x amplified signal output in V versus microplastic concentration. Each data series represents a different solution concentration of Nile Red. Compared to the unamplified data, 100x amplification introduces noticeable noise for NR concentrations of 1 ug/mL and 2 ug/mL. Given the increased noise in the amplified data and the similar linear trend lines across amplification settings, an external amplifier such as the SR560 pre-amplifier may not be necessary or can be substituted for a transimpedance amplifier circuit.

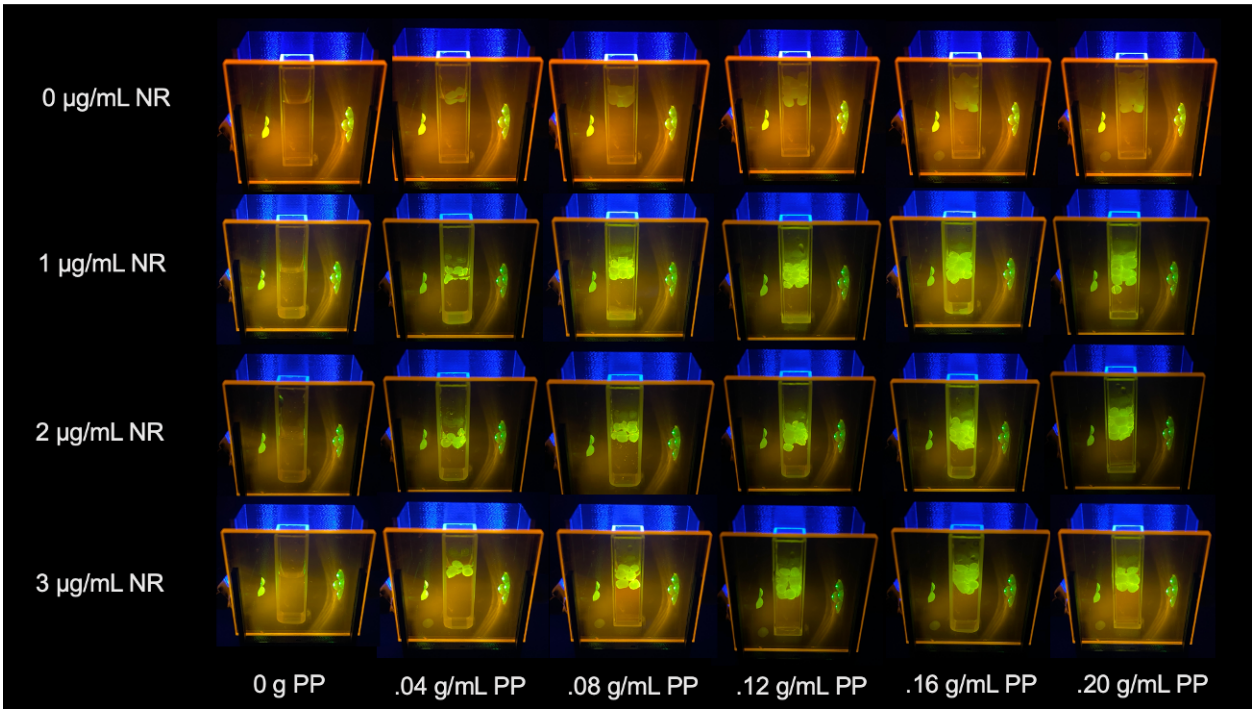

Figure 4.7: Control and fluorescing test solutions for various microplastic and Nile Red concentrations. Little yellow-green fluorescent light can be seen in control solutions, even with higher MP concentrations. The 1 ug/mL and 2 ug/mL solutions present similar visual fluorescence characteristics. The 3 ug/mL is generally brighter across each MP concentration. A slight red tinge can also be seen in these solutions due to excess dye in the liquid sample.

4.4 Conclusions and Future Work

While the preliminary prototype of the system holds promise to quantify in situ larger microplastics (especially plastic pollution in the form of nurdles or virgin pellets), the system is still constrained by several factors that can be improved upon in future work. One such issue is the sensitivity of the current system to MP positioning in the cuvette.

In this experimental set-up, the lens and photodiode were positioned such that the water surface in the cuvette was aligned with the center plane of the lens and the photodiode. Given that polypropylene floats on water surfaces, the fluorescent emissions from the MPs were optimally positioned to be captured by the photodiode. However, environmental samples will contain plastics of different densities and be distributed throughout the sample. The system should either be redesigned to accommodate plastics of varying densities or constrained only to plastics of similar densities.

Additionally, mixed plastics or field samples were not tested in this study, indicating the current iteration of the system will likely not distinguish between different polymers or organic material that easily uptakes Nile Red. Given the spectral data presented in Chapter 2, an array of photodiodes with varying responsivity peaks for MP detection may distinguish between different polymers or materials. However, a separate method will likely need to differentiate between plastics and non-plastics, given that many organic materials exhibit similar spectral peaks to Nile Red-stained plastics.

Other factors, such as optimal staining protocols and Nile Red solvent, should be rigorously investigated. Given that plastics stained with Nile Red emit a range of wavelengths based on the excitation light, more comprehensive spectroscopy research should be undertaken to understand excitation and emission characteristics specifically for in situ samples containing mixed plastics. Furthermore, increase in dye concentration leads to faint fluorescence of the liquid sample itself, which may mask other important spectra. In the future, a quenching procedure to reduce liquid fluorescence such as one described by Park et. al

(2022) should be implemented [13].

In contrast to Chapter 3, this chapter presented the design and testing of a proof-of-concept for a low-cost system intended to rapidly detect larger microplastics within in situ samples. While certain aspects of the work hold promise, future iterations of this system need to address (1) perform rigorous validation of this technique for polypropylene field samples (2) incorporate polymer identification in the photodiode array selection (2) explore different system geometries that accommodates detection of microplastics with varying densities (3) quench fluorescence within the liquid sample to reduce optical interference with critical spectral peaks from MPs (4) determine an optimal staining protocol that maximizes fluorescence intensity of plastic samples but reduces absorption by biological material.

Chapter 5

Summary, Conclusions, and Prognosis

This thesis explored several different optical detection methods for Nile Red-stained plastics with a push toward developing low-cost, accessible microplastic monitoring systems. Summaries and conclusions are discussed.

5.1 Fluorescence Emission Spectra for Nile Red stained Plastics

The fluorescence emission spectra dataset successfully provided a preliminary basis for distinguishing between stained polymers using spectral data alone. Incorporating higher-resolution data capture may decrease the spectral overlap between plastic and organic materials, allowing for further categorization possibilities.

Future work includes building a larger dataset and training a model to identify the polymer of plastic based on spectral data. Additional excitation wavelengths should also be tested to investigate the possibility of other emission peaks. Overall, this work built the foundation for the future development of a rapid, automated microplastic detection and polymer identification method.

5.2 Pairing spectral data with a low-cost microplastic imaging configuration for rapid polymer identification

This work successfully captured images of microplastics and paired them with their spectral data for various excitation wavelengths and filter combinations. The images presented within the chapter show clear visual distinction between polymers, qualitatively validating the spectral data. Future work can expand this dataset and train a model to image and classify microplastics in real-time.

5.3 Utilizing low-cost photodiodes for microplastic detection in liquid samples

This work explored the feasibility of using low-cost photodiodes to detect microplastics in liquid samples. The preliminary results from laboratory tests indicated a linear relationship between the system's output and the concentration of microplastics in the test solutions. However, further validation needs to be done. This proof-of-concept demonstrated the potential for developing an inexpensive, field-deployable system for in situ microplastic detection.

5.4 Final Conclusion

This work provides several pathways to develop rapid microplastic detection models capable of distinguishing between polymer types that can be deployed on low-cost, field portable systems.

Appendix A

Fourier Transform Infrared Spectroscopy (FTIR) Results for Polymer Validation

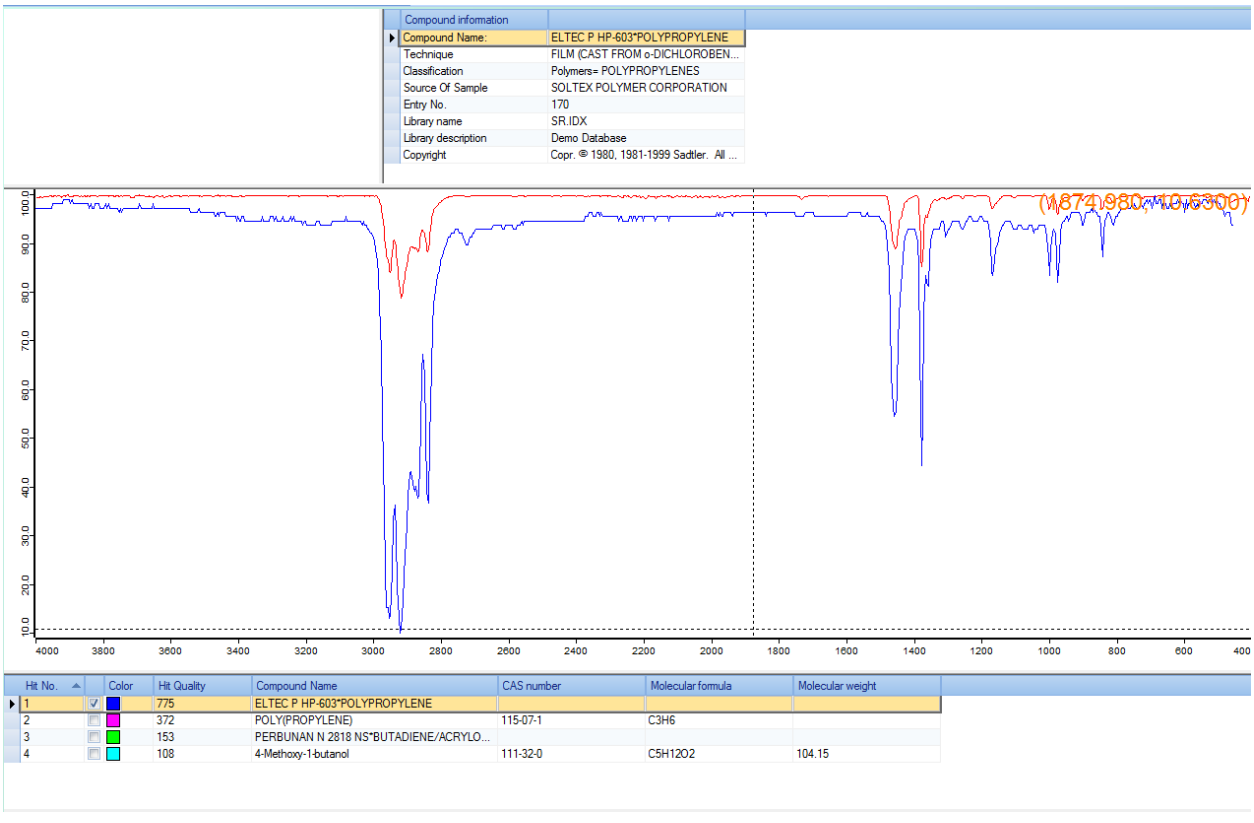

Figure A.1: FTIR spectra for polypropylene

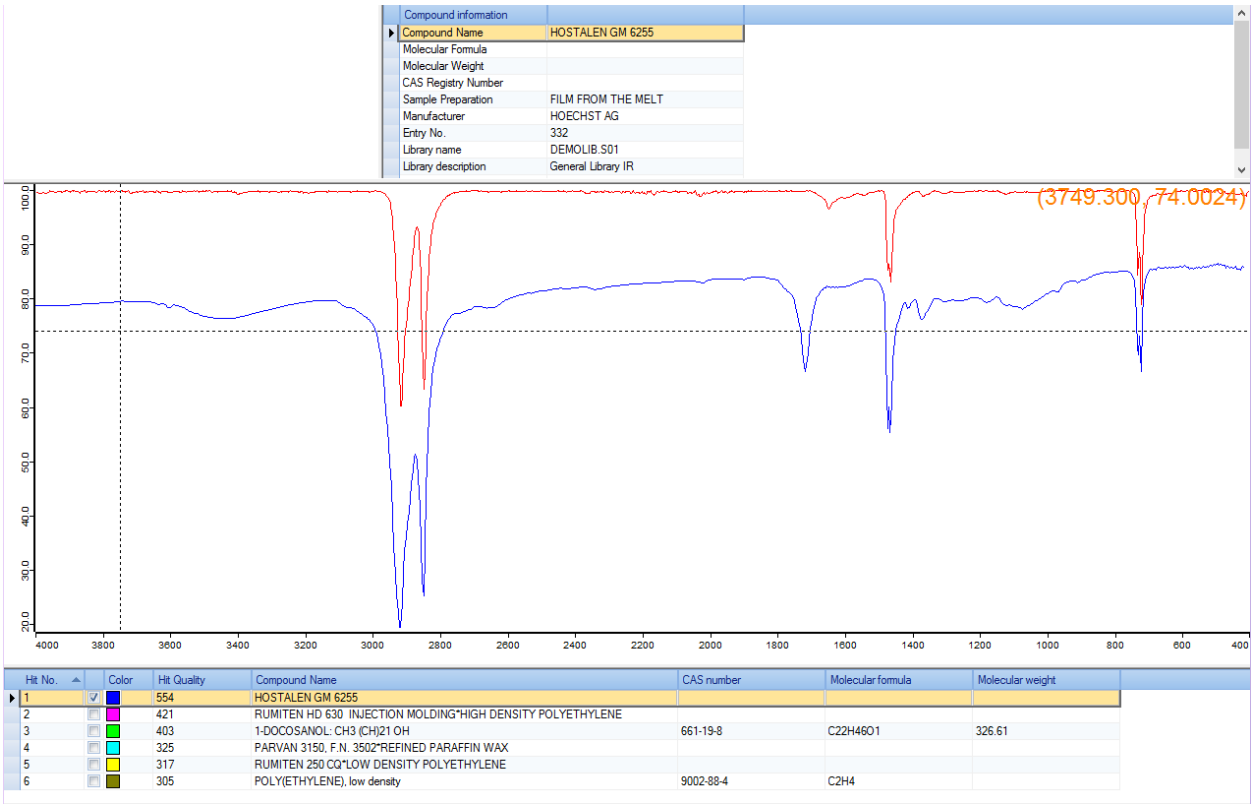

Figure A.2: FTIR spectra for polyethylene

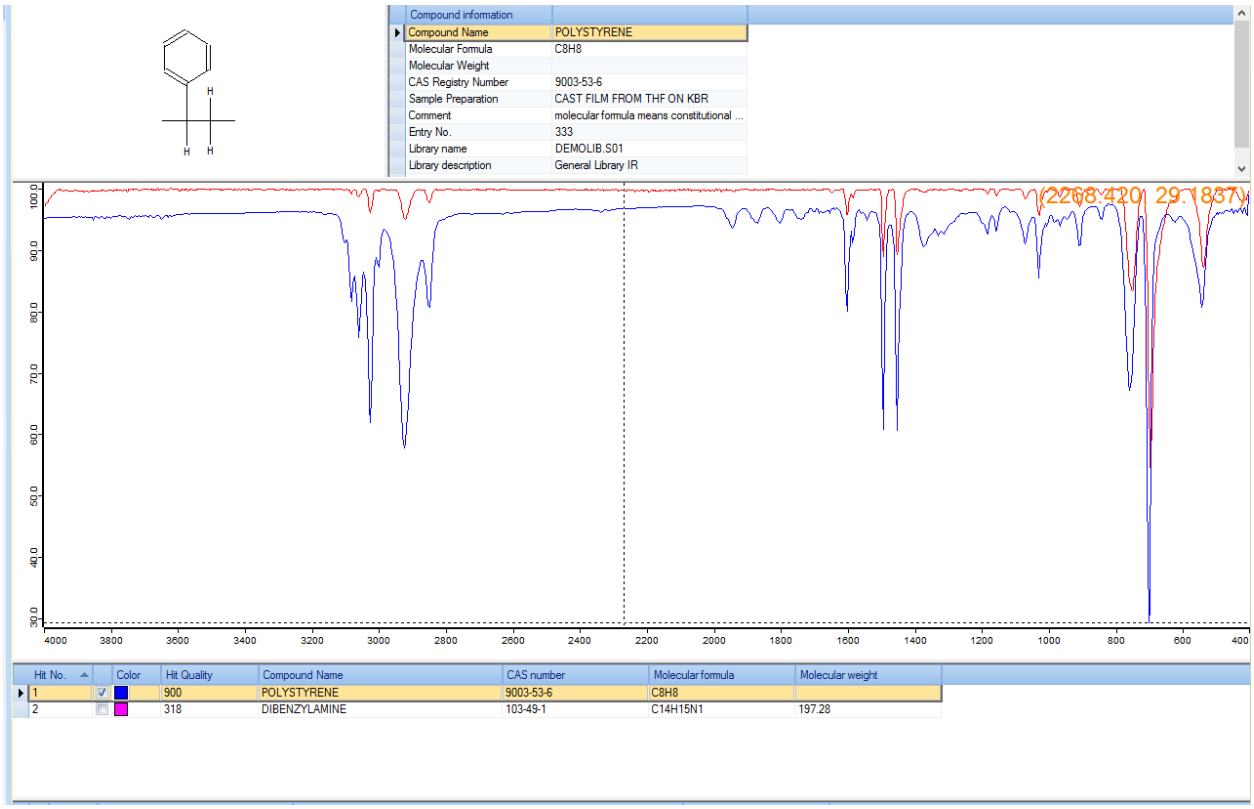

Figure A.3: FTIR spectra for polystyrene

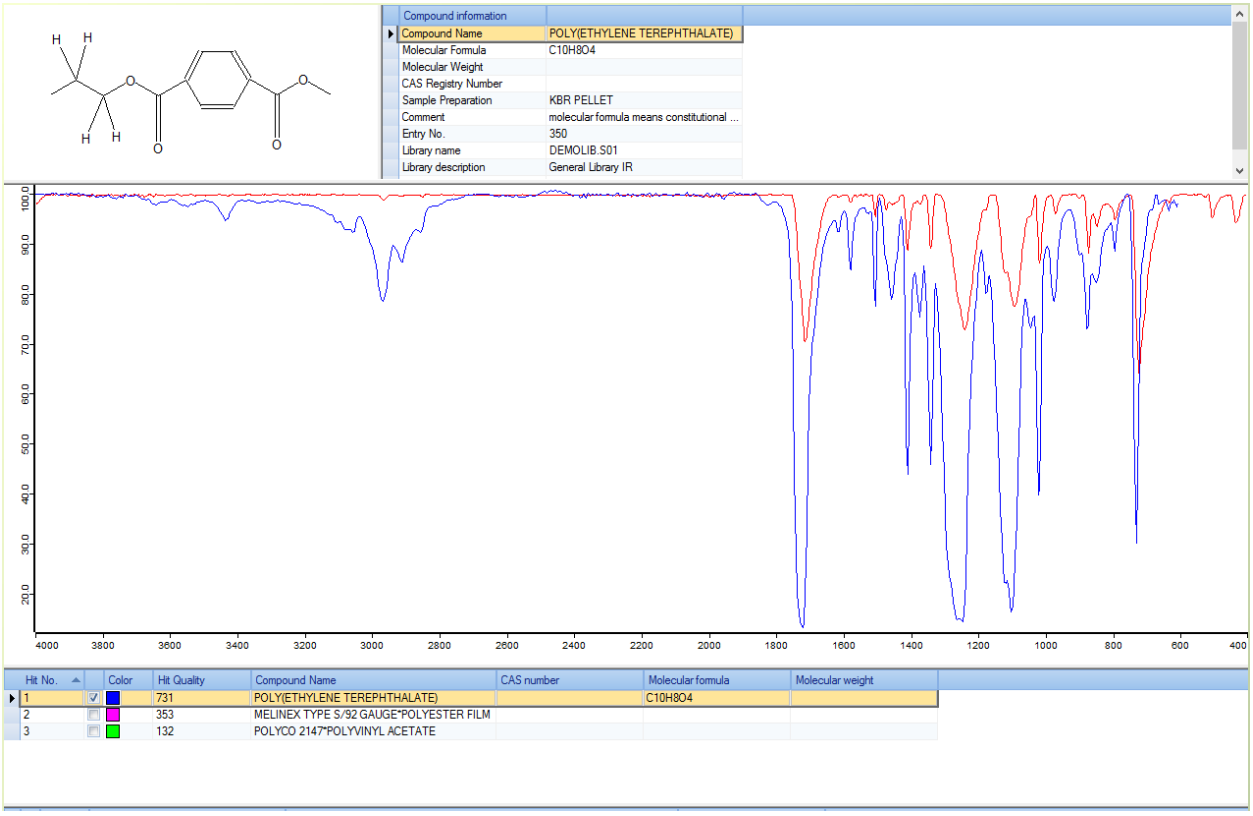

Figure A.4: FTIR spectra for polyester

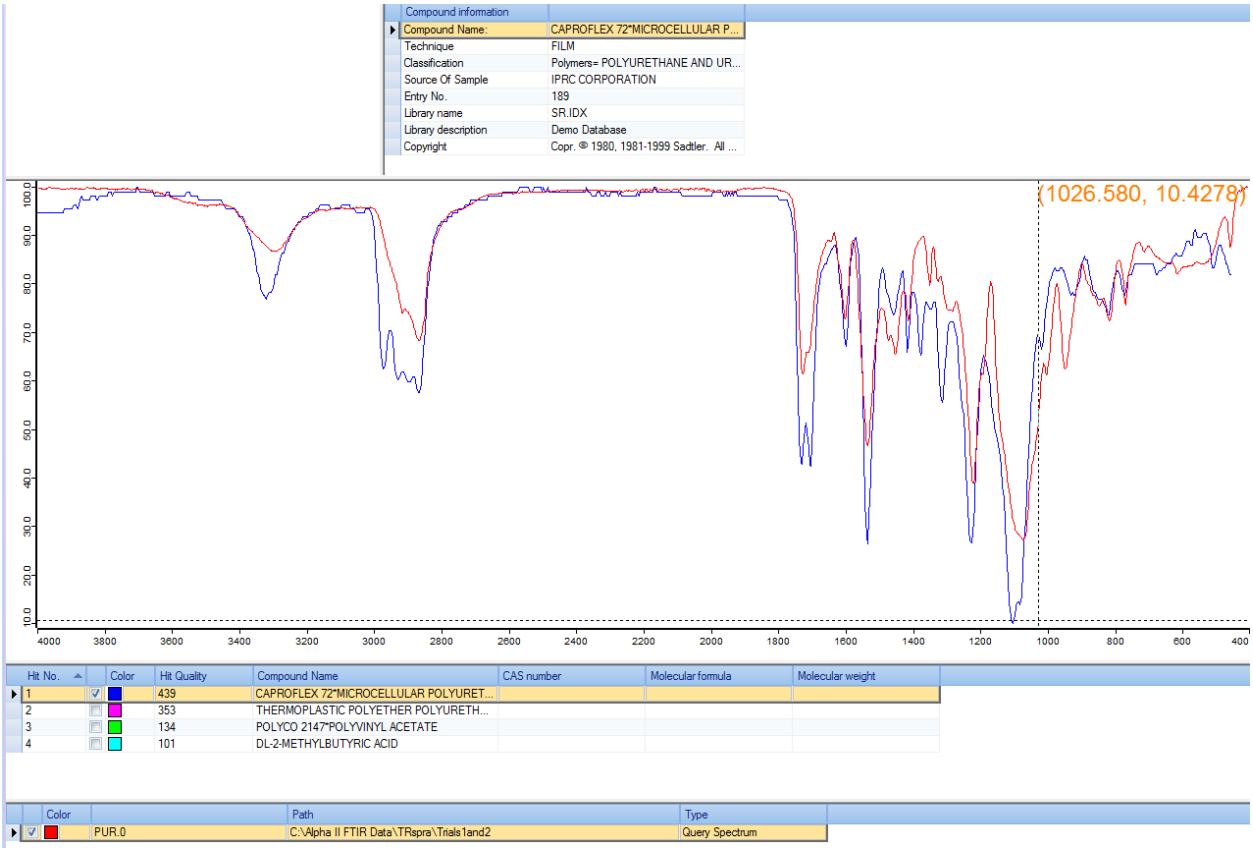

Figure A.5: FTIR spectra for polyurethane

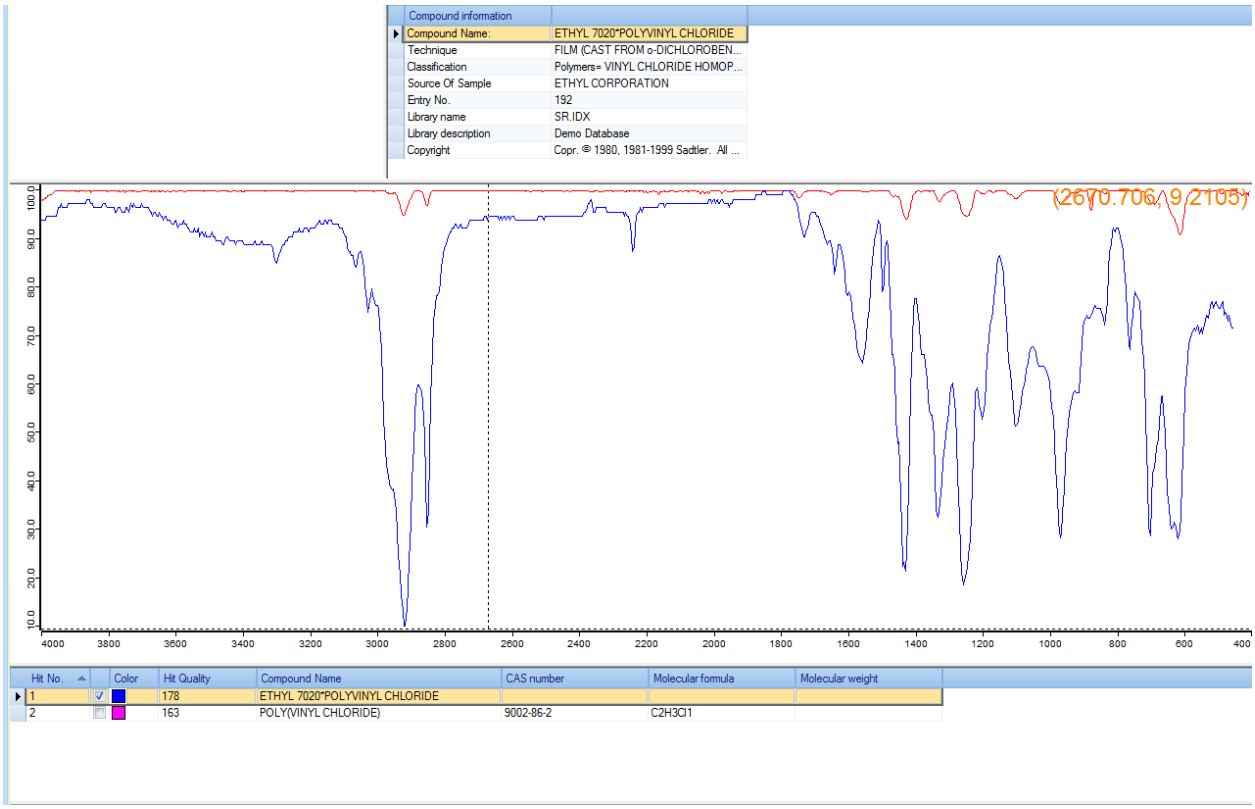

Figure A.6: FTIR spectra for polyvinyl chloride

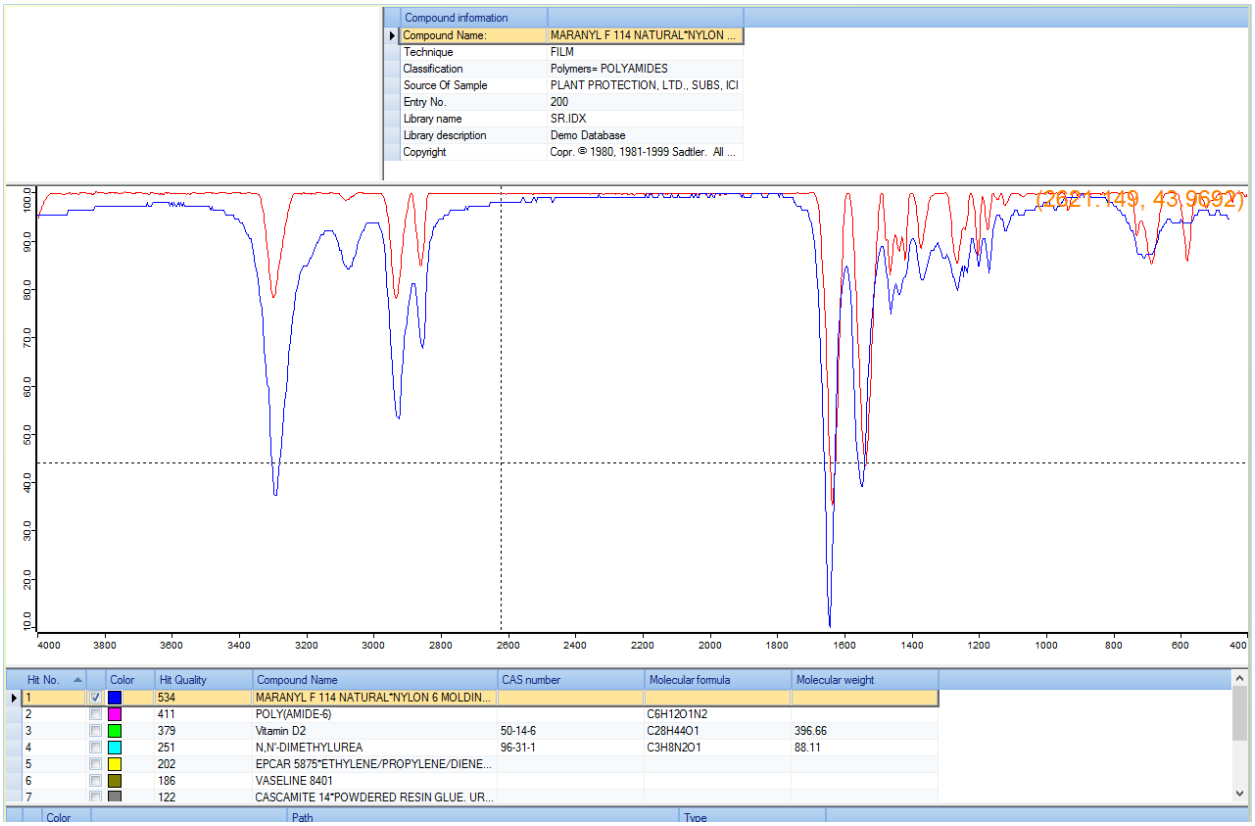

Figure A.7: FTIR spectra for nylon

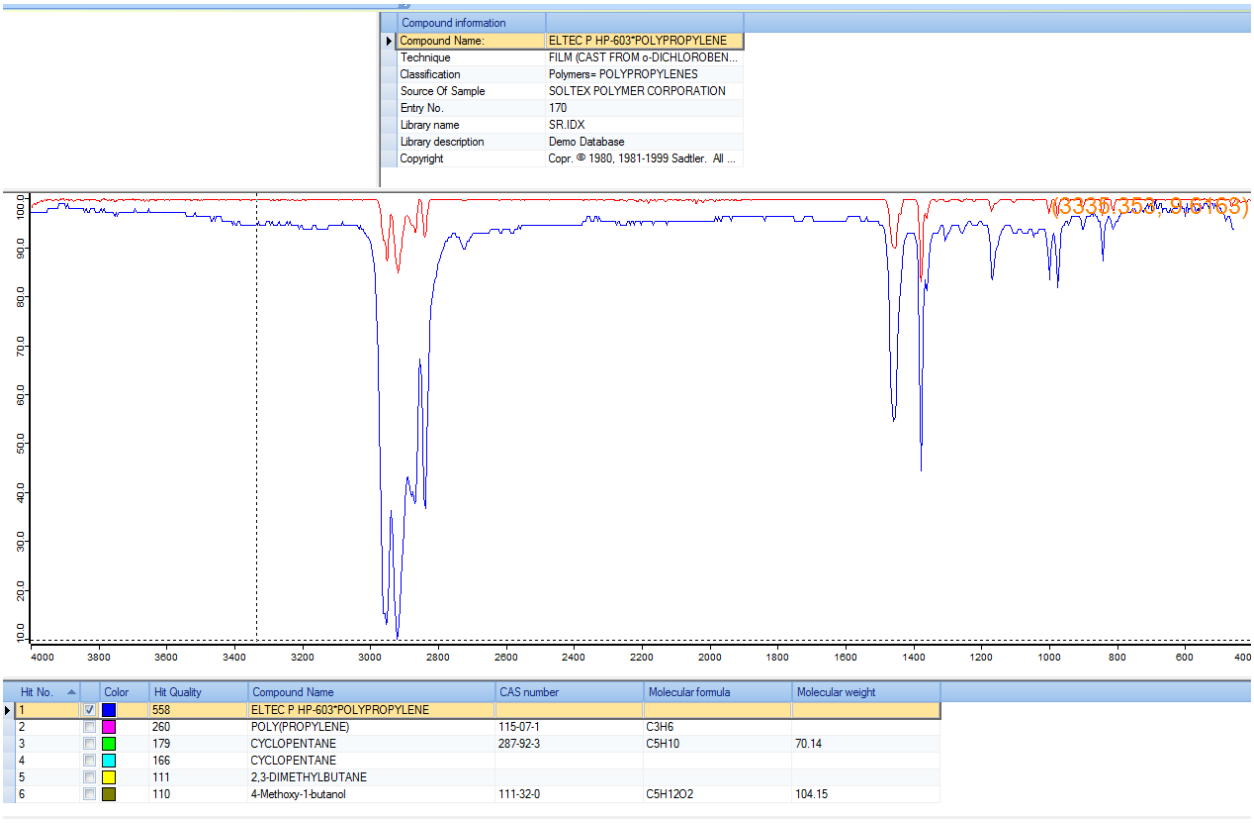

Figure A.8: FTIR spectra for polypropylene field sample 1

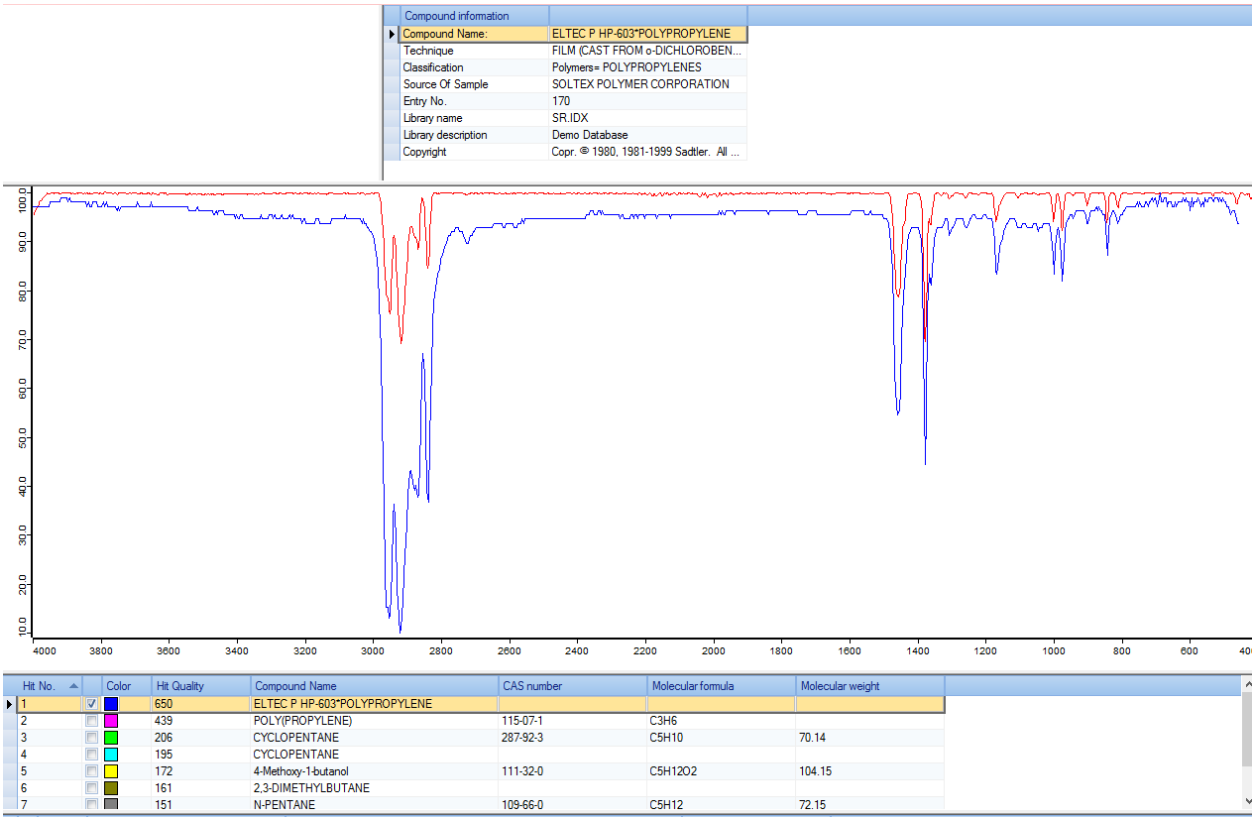

Figure A.9: FTIR spectra for polypropylene field sample 2

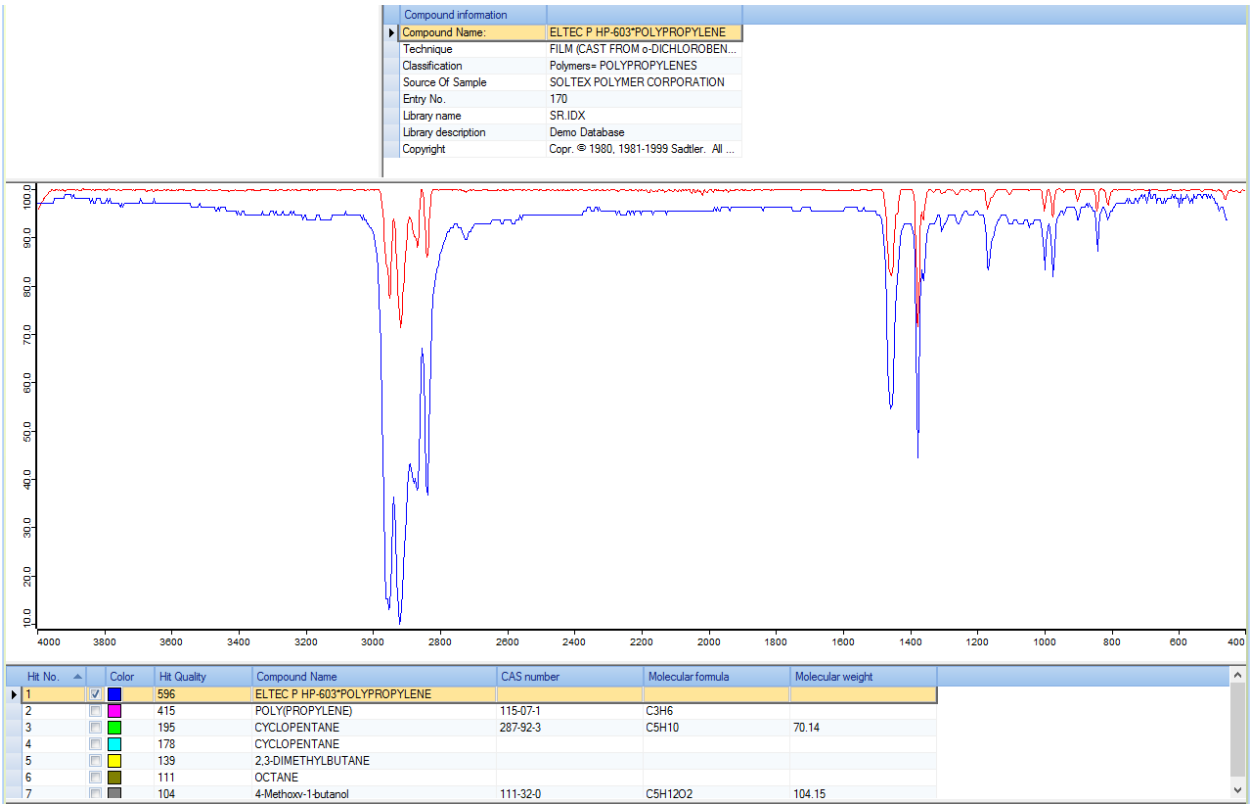

Figure A.10: FTIR spectra for polypropylene field sample 3

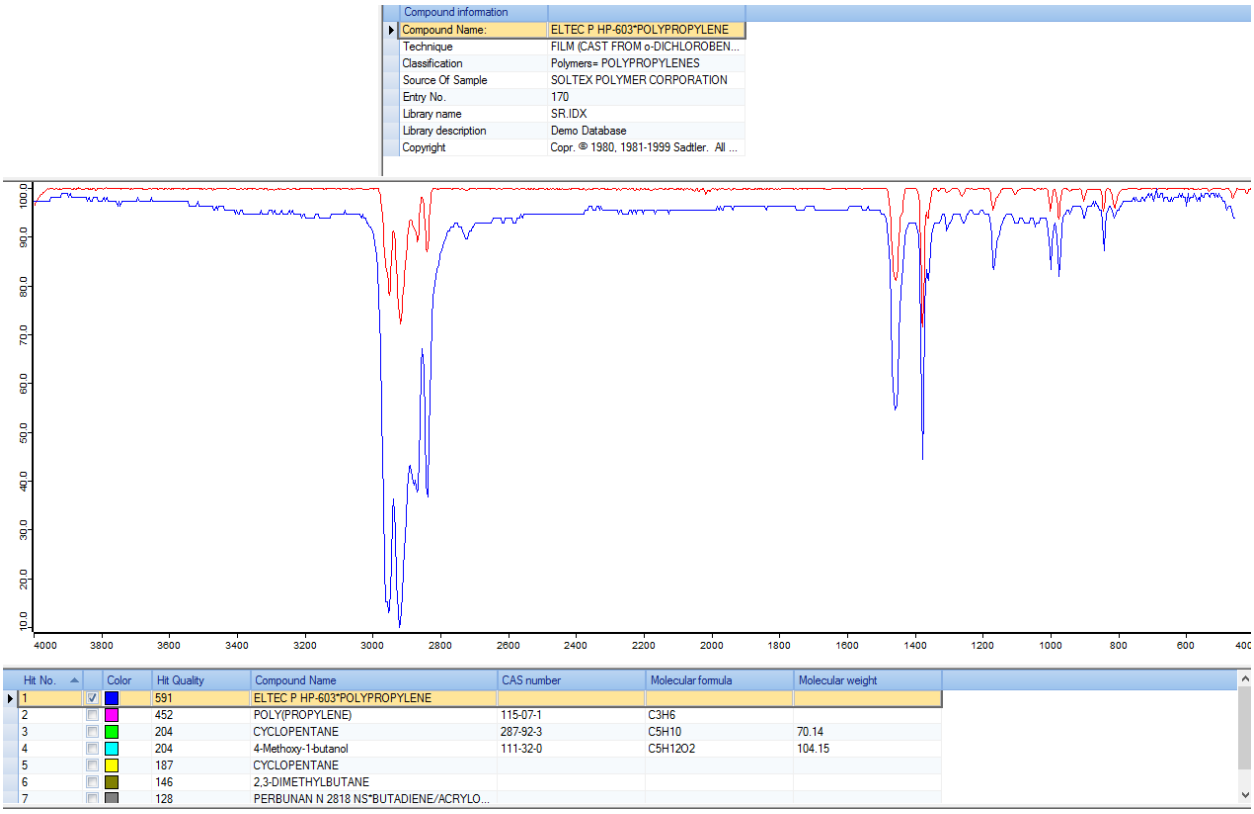

Figure A.11: FTIR spectra for polypropylene field sample 4

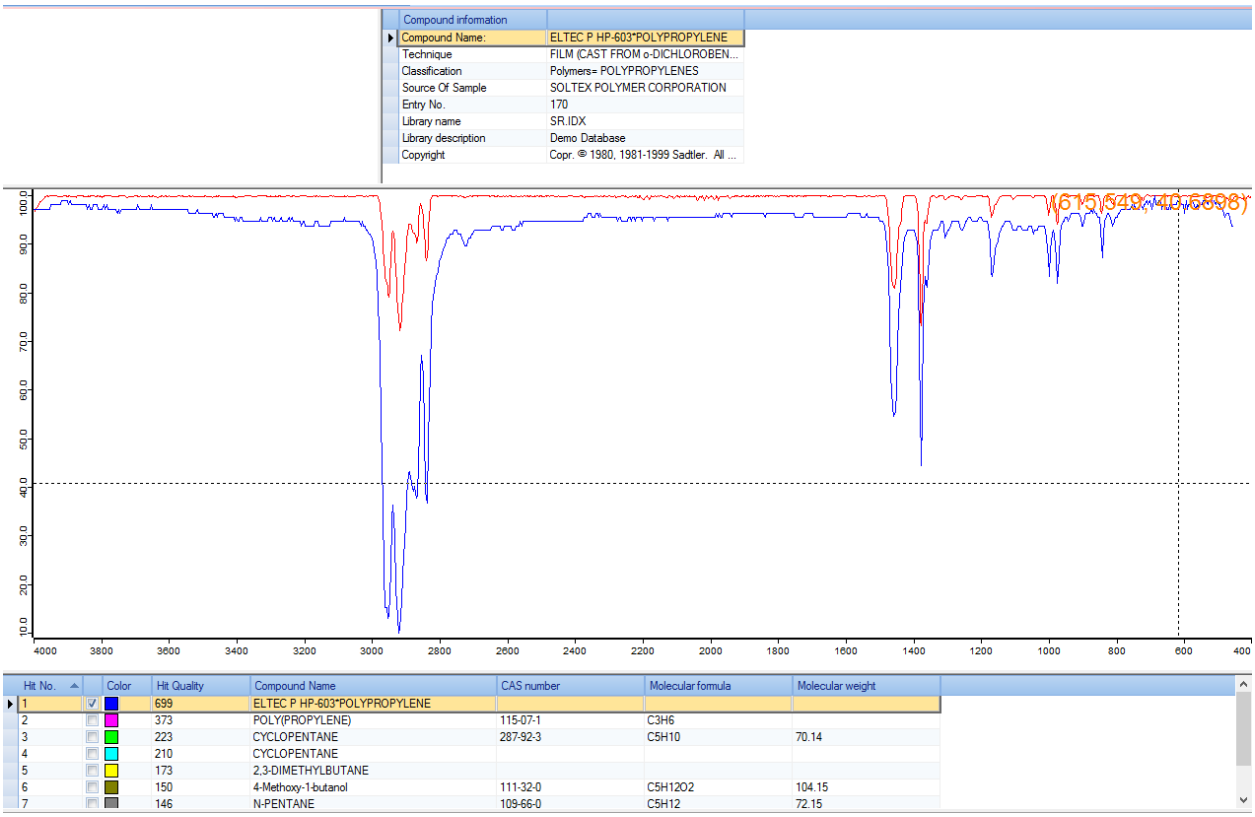

Figure A.12: FTIR spectra for polypropylene field sample 5

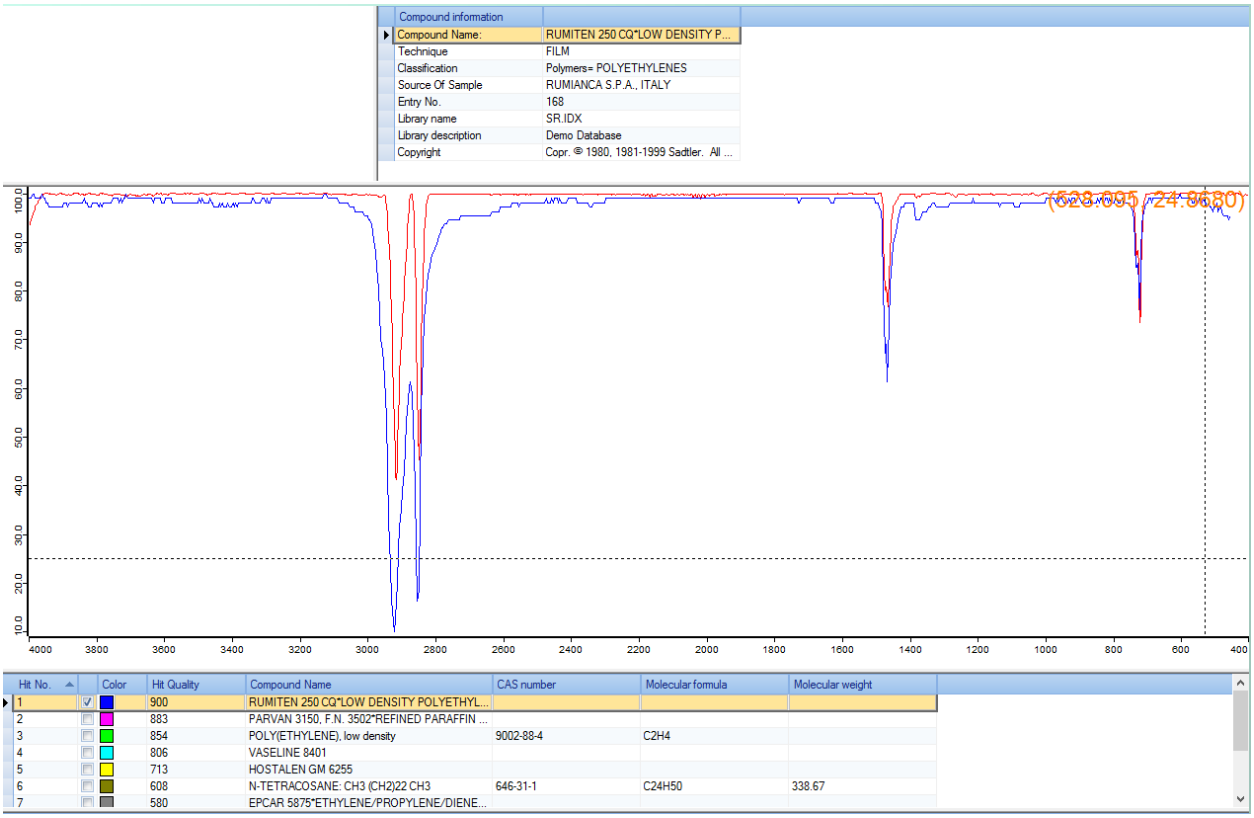

Figure A.13: FTIR spectra for polyethylene field sample 1

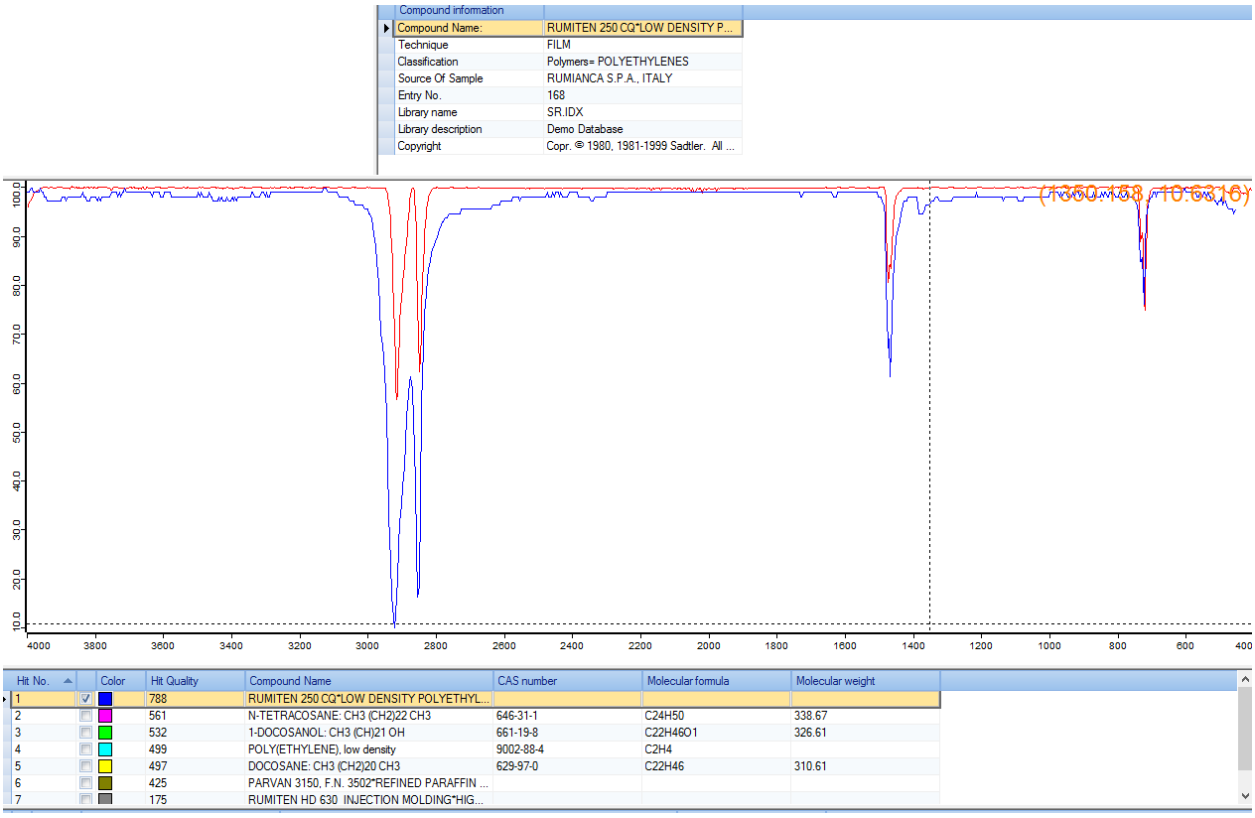

Figure A.14: FTIR spectra for polyethylene field sample 2

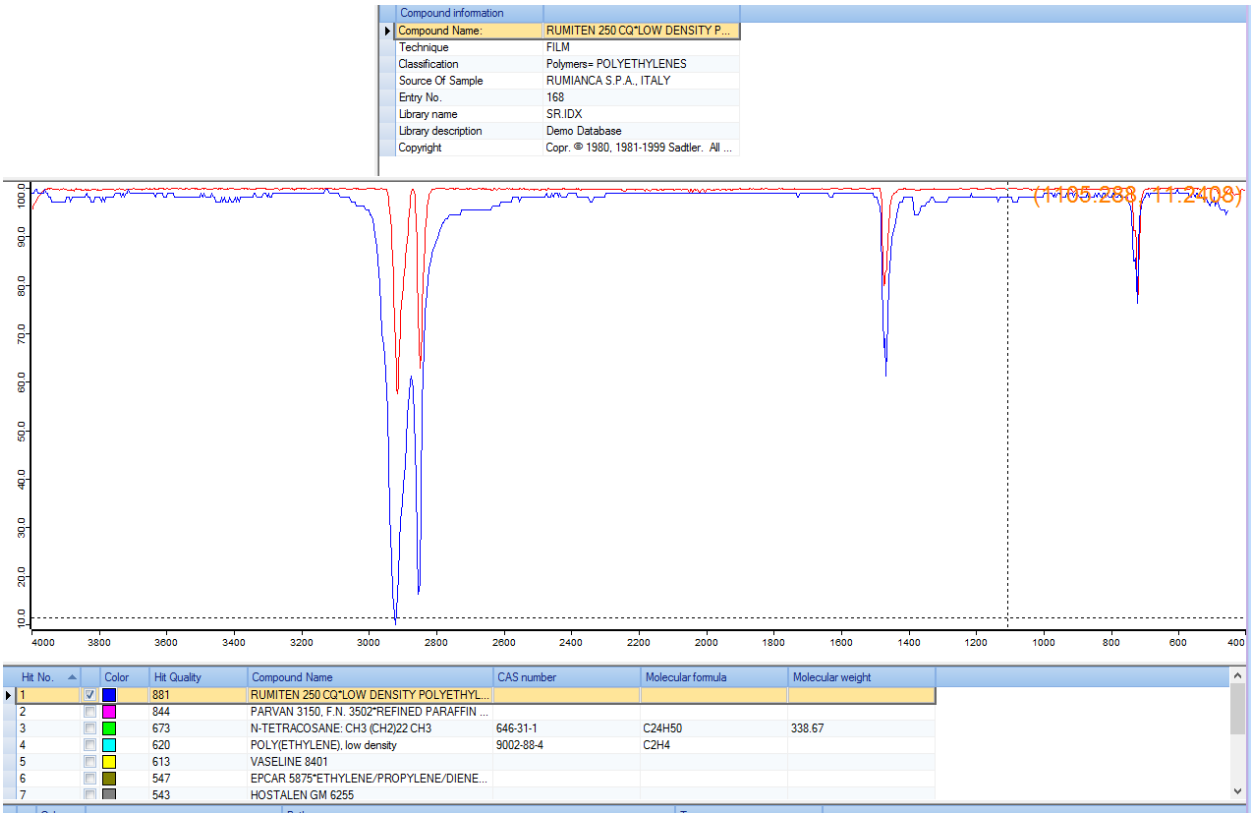

Figure A.15: FTIR spectra for polyethylene field sample 3

References

[1] OECD, *Global Plastics Outlook: Policy Scenarios to 2060*. Paris: Organisation for Economic Co-operation and Development, 2022. URL: https://www.oecd-ilibrary.org/environment/global-plastics-outlook_aa1edf33-en (visited on 05/20/2024).

[2] T. Y. Suman, W.-G. Li, S. Alif, V. R. P. Faris, D. J. Amarnath, J.-G. Ma, and D.-S. Pei, "Characterization of petroleum-based plastics and their absorbed trace metals from the sediments of the marina beach in chennai, india," *Environmental Sciences Europe*, vol. 32, no. 1, p. 110, Aug. 27, 2020, ISSN: 2190-4715. DOI: 10.1186/s12302-020-00388-5. URL: https://doi.org/10.1186/s12302-020-00388-5 (visited on 05/20/2024).

[3] "The plastic pollution crisis - story | IUCN." (), URL: https://www.iucn.org/story/202207/plastic-pollution-crisis (visited on 05/06/2024).

[4] N. Fisheries. "Deepwater horizon 10 years later: 10 questions | NOAA fisheries," NOAA. Archive Location: Southeast,National. (Jan. 6, 2021), URL: https://www.fisheries.noaa.gov/news/deepwater-horizon-10-years-later-10-questions (visited on 05/20/2024).

[5] Z. Huang, B. Hu, and H. Wang, "Analytical methods for microplastics in the environment: A review," *Environmental Chemistry Letters*, vol. 21, no. 1, pp. 383–401, 2023, ISSN: 1610-3653. DOI: 10.1007/s10311-022-01525-7. URL: https://www.ncbi.nlm.nih.gov/pmc/articles/PMC9521859/ (visited on 05/20/2024).

[6] T. Maes, R. Jessop, N. Wellner, K. Haupt, and A. G. Mayes, "A rapid-screening approach to detect and quantify microplastics based on fluorescent tagging with nile red,"

Scientific Reports, vol. 7, no. 1, p. 44 501, Mar. 16, 2017, Publisher: Nature Publishing Group, ISSN: 2045-2322. DOI: 10.1038/srep44501. URL: https://www.nature.com/articles/srep44501 (visited on 05/16/2024).

[7] A. Bianco, L. Carena, N. Peitsaro, F. Sordello, D. Vione, and M. Passananti, "Rapid detection of nanoplastics and small microplastics by nile-red staining and flow cytometry," *Environmental Chemistry Letters*, vol. 21, no. 2, pp. 647–653, Apr. 1, 2023, ISSN: 1610-3661. DOI: 10.1007/s10311-022-01545-3. URL: https://doi.org/10.1007/s10311-022-01545-3 (visited on 05/20/2024).

[8] N. Meyers, A. I. Catarino, A. M. Declercq, A. Brenan, L. Devriese, M. Vandegehuchte, B. De Witte, C. Janssen, and G. Everaert, "Microplastic detection and identification by nile red staining: Towards a semi-automated, cost- and time-effective technique," *Science of The Total Environment*, vol. 823, p. 153 441, Jun. 1, 2022, ISSN: 0048-9697. DOI: 10.1016/j.scitotenv.2022.153441. URL: https://www.sciencedirect.com/science/article/pii/S0048969722005332 (visited on 05/19/2024).

[9] M. T. Sturm, E. Myers, D. Schober, A. Korzin, and K. Schuhen, "Development of an inexpensive and comparable microplastic detection method using fluorescent staining with novel nile red derivatives," *Analytica*, vol. 4, no. 1, pp. 27–44, Mar. 2023, Number: 1 Publisher: Multidisciplinary Digital Publishing Institute, ISSN: 2673-4532. DOI: 10.3390/analytica4010004. URL: https://www.mdpi.com/2673-4532/4/1/4 (visited on 05/19/2024).

[10] S. Chatterjee, E. Krolis, R. Molenaar, M. M. A. E. Claessens, and C. Blum, "Nile red staining for nanoplastic quantification: Overcoming the challenge of false positive counts due to fluorescent aggregates," *Environmental Challenges*, vol. 13, p. 100 744, Dec. 1, 2023, ISSN: 2667-0100. DOI: 10.1016/j.envc.2023.100744. URL: https://www.sciencedirect.com/science/article/pii/S2667010023000689 (visited on 05/17/2024).

[11] W. J. Shim, Y. K. Song, S. H. Hong, and M. Jang, "Identification and quantification of microplastics using nile red staining," *Marine Pollution Bulletin*, vol. 113, no. 1, pp. 469–476, Dec. 15, 2016, ISSN: 0025-326X. DOI: 10.1016/j.marpolbul.2016.10.049. URL: https://www.sciencedirect.com/science/article/pii/S0025326X16308669 (visited on 05/17/2024).

[12] F. Ruggero, R. Gori, and C. Lubello, "Methodologies for microplastics recovery and identification in heterogeneous solid matrices: A review," *Journal of Polymers and the Environment*, vol. 28, no. 3, pp. 739–748, Mar. 1, 2020, ISSN: 1572-8919. DOI: 10.1007/s10924-019-01644-3. URL: https://doi.org/10.1007/s10924-019-01644-3 (visited on 05/17/2024).

[13] D. H. Park, S. B. Oh, and S. C. Hong, "In situ fluorescent illumination of microplastics in water utilizing a combination of dye/surfactant and quenching techniques," *Polymers*, vol. 14, no. 15, p. 3084, Jan. 2022, Number: 15 Publisher: Multidisciplinary Digital Publishing Institute, ISSN: 2073-4360. DOI: 10.3390/polym14153084. URL: https://www.mdpi.com/2073-4360/14/15/3084 (visited on 05/17/2024).

[14] T. Stanton, M. Johnson, P. Nathanail, R. L. Gomes, T. Needham, and A. Burson, "Exploring the efficacy of nile red in microplastic quantification: A costaining approach," *Environmental Science & Technology Letters*, vol. 6, no. 10, pp. 606–611, Oct. 8, 2019, Publisher: American Chemical Society. DOI: 10.1021/acs.estlett.9b00499. URL: https://doi.org/10.1021/acs.estlett.9b00499 (visited on 05/06/2024).

[15] H. Maxwell S, F. Melinda K, and G. Matthew, "Counterstaining to separate nile red-stained microplastic particles from terrestrial invertebrate biomass," *Environmental Science & Technology*, vol. 54, no. 9, pp. 5580–5588, May 5, 2020, Publisher: American Chemical Society, ISSN: 0013-936X. DOI: 10.1021/acs.est.0c00711. URL: https://doi.org/10.1021/acs.est.0c00711 (visited on 05/06/2024).

[16] A. Käppler, D. Fischer, S. Oberbeckmann, G. Schernewski, M. Labrenz, K.-J. Eichhorn, and B. Voit, "Analysis of environmental microplastics by vibrational microspectroscopy: FTIR, raman or both?" *Analytical and Bioanalytical Chemistry*, vol. 408, no. 29, pp. 8377–8391, Nov. 2016, ISSN: 1618-2650. DOI: 10.1007/s00216-016-9956-3.

[17] S. Konde, S. Brackmann, J. Prume, M. Gerhard, and M. Koch, *Nile red staining for the detection of microplastics: A comprehensive study on the emission spectra*, ISSN: 2693-5015, Feb. 16, 2023. DOI: 10.21203/rs.3.rs-2579237/v1. URL: https://www.researchsquare.com/article/rs-2579237/v1 (visited on 05/16/2024).

[18] J. C. Prata, J. P. da Costa, I. Lopes, A. C. Duarte, and T. Rocha-Santos, "Effects of microplastics on microalgae populations: A critical review," *The Science of the Total Environment*, vol. 665, pp. 400–405, May 15, 2019, ISSN: 1879-1026. DOI: 10.1016/j.scitotenv.2019.02.132.

[19] M. T. Sturm, H. Horn, and K. Schuhen, "The potential of fluorescent dyes—comparative study of nile red and three derivatives for the detection of microplastics," *Analytical and Bioanalytical Chemistry*, vol. 413, no. 4, pp. 1059–1071, Feb. 1, 2021, ISSN: 1618-2650. DOI: 10.1007/s00216-020-03066-w. URL: https://doi.org/10.1007/s00216-020-03066-w (visited on 05/16/2024).

[20] H. Aoki, "Material-specific determination based on microscopic observation of single microplastic particles stained with fluorescent dyes," *Sensors*, vol. 22, no. 9, p. 3390, Jan. 2022, Number: 9 Publisher: Multidisciplinary Digital Publishing Institute, ISSN: 1424-8220. DOI: 10.3390/s22093390. URL: https://www.mdpi.com/1424-8220/22/9/3390 (visited on 05/16/2024).

[21] D. Ho, S. Liu, H. Wei, and K. G. Karthikeyan, "The glowing potential of nile red for microplastics identification: Science and mechanism of fluorescence staining," *Microchemical Journal*, vol. 197, p. 109 708, Feb. 1, 2024, ISSN: 0026-265X. DOI: 10.1016/

j.microc.2023.109708. URL: https://www.sciencedirect.com/science/article/pii/S0026265X23013279 (visited on 05/17/2024).

[22] S. Gies, E.-M. Schömann, J. Anna Prume, and M. Koch, "Exploring the potential of time-resolved photoluminescence spectroscopy for the detection of plastics," *Applied Spectroscopy*, vol. 74, no. 9, pp. 1161–1166, Sep. 1, 2020, Publisher: SAGE Publications Ltd STM, ISSN: 0003-7028. DOI: 10.1177/0003702820933282. URL: https://doi.org/10.1177/0003702820933282 (visited on 05/16/2024).

[23] B. Lotter, S. Konde, J. Nguyen, M. Grau, M. Koch, and P. Lenz, "Identifying plastics with photoluminescence spectroscopy and machine learning," *Scientific Reports*, vol. 12, no. 1, p. 18 840, Nov. 6, 2022, Publisher: Nature Publishing Group, ISSN: 2045-2322. DOI: 10.1038/s41598-022-23414-3. URL: https://www.nature.com/articles/s41598-022-23414-3 (visited on 05/16/2024).

[24] S. Konde, J. Ornik, J. A. Prume, J. Taiber, and M. Koch, "Exploring the potential of photoluminescence spectroscopy in combination with nile red staining for microplastic detection," *Marine Pollution Bulletin*, vol. 159, p. 111 475, Oct. 1, 2020, ISSN: 0025-326X. DOI: 10.1016/j.marpolbul.2020.111475. URL: https://www.sciencedirect.com/science/article/pii/S0025326X20305932 (visited on 05/17/2024).

[25] Granite. "What are absorption, excitation and emission spectra?" Edinburgh Instruments. (), URL: https://www.edinst.com/blog/what-are-absorption-excitation-and-emission-spectra/ (visited on 05/16/2024).

[26] J. Ornik, S. Sommer, S. Gies, M. Weber, C. Lott, J. C. Balzer, and M. Koch, "Could photoluminescence spectroscopy be an alternative technique for the detection of microplastics? first experiments using a 405 nm laser for excitation," *Applied Physics B*, vol. 126, no. 1, p. 15, Dec. 18, 2019, ISSN: 1432-0649. DOI: 10.1007/s00340-019-7360-3. URL: https://doi.org/10.1007/s00340-019-7360-3 (visited on 05/17/2024).

[27] S. Prasad, K. Bennett, A. Bennett, and M. Triantafyllou, "Towards a low-cost, rapid microplastic optical detection system using fluorescent staining through nile red for in situ ocean deployment," in *OCEANS 2023 - Limerick*, Jun. 2023, pp. 1–5. DOI: 10.1109/OCEANSLimerick52467.2023.10244433. URL: https://ieeexplore.ieee.org/document/10244433/citations#citations (visited on 05/20/2024).

[28] T. M. Karlsson, L. Arneborg, G. Broström, B. C. Almroth, L. Gipperth, and M. Hassellöv, "The unaccountability case of plastic pellet pollution," *Marine Pollution Bulletin*, vol. 129, no. 1, pp. 52–60, Apr. 1, 2018, ISSN: 0025-326X. DOI: 10.1016/j.marpolbul.2018.01.041. URL: https://www.sciencedirect.com/science/article/pii/S0025326X18300523 (visited on 05/20/2024).

[29] J. C. Prata, "Influence of intrinsic plastics characteristics on nile red staining and fluorescence," *Journal of Sea Research*, vol. 195, p. 102 431, Oct. 1, 2023, ISSN: 1385-1101. DOI: 10.1016/j.seares.2023.102431. URL: https://www.sciencedirect.com/science/article/pii/S1385110123001004 (visited on 05/20/2024).

[30] M. R. Gregory, "Accumulation and distribution of virgin plastic granules on new zealand beaches," *New Zealand Journal of Marine and Freshwater Research*, vol. 12, no. 4, pp. 399–414, Dec. 1978, ISSN: 0028-8330, 1175-8805. DOI: 10.1080/00288330.1978.9515768. URL: http://www.tandfonline.com/doi/abs/10.1080/00288330.1978.9515768 (visited on 05/20/2024).